Zeitschrift: Schweizerische mineralogische und petrographische Mitteilungen = Bulletin suisse de minéralogie et pétrographie

Band: 82 (2002)

Heft: 3

Artikel: Thermobarometry in eclogites with multipe stages of mineral growth : an example from the Sesia-Lanzo Zone (Western Alps, Italy)

Autor: Tropper, Peter / Essene, Eric J.

DOI: https://doi.org/10.5169/seals-62377

SCHWEIZ. MINERAL. PETROGR. MITT. 82, 487–514, 2002

Thermobarometry in eclogites with multiple stages of mineral growth: an example from the Sesia-Lanzo Zone (Western Alps, Italy)

by *Peter Tropper*[1,2] and *Eric J. Essene*[2]

Abstract

Eclogites of the Ianca Valley in northern Italy underwent Eo-Alpine eclogite-facies metamorphism and subsequent retrogression under blueschist- and greenschist-facies conditions, which led to the formation of a sequence of mineral assemblages. A first eclogite-facies assemblage (high-pressure stage I: paragonite + clinozoisite + zoisite + garnet + kyanite + quartz) is preserved in the cores of some garnets. Inclusion assemblages in garnet rims represent two further stages in the eclogite-facies: (1) a first stage has the assemblage omphacite + clinozoisite + garnet + kyanite + rutile + quartz ± zoisite (high-pressure stage II) and (2) a second stage with the assemblage omphacite + barroisite + rutile + quartz + zircon (high-pressure stage III) is occasionally found in the outermost rims. The latter assemblage represents hydration in the eclogite-facies, which also led to the formation of the matrix assemblage barroisite + omphacite + garnet + clinozoisite + paragonite + muscovite + dolomite + rutile + quartz ± zoisite, without kyanite. Hydration continued, forming veins crosscutting the main foliation with the assemblage paragonite + clinozoisite + zoisite + barroisite + quartz ± omphacite. During a subsequent blueschist-facies event, glaucophane appeared, and finally, a greenschist-facies assemblage actinolite + chlorite + clinozoisite + muscovite + talc + albite + titanite + calcite + quartz formed. The successive mineral assemblages were used to construct a *P-T* path, yielding a decompression path from the eclogite-facies from 550–650 °C, 17–21 kbar (high-pressure stages I and II) to 520–650 °C, 16–21 kbar (high-pressure stage III) and 400–500 °C and 8–10 kbar in the blueschist-facies. The conditions of the greenschist-facies are around 250–350 °C and 3–6 kbar. In addition, an attempt was made to characterize the evolution of $a(H_2O)$ during the *P-T* path. The activity of the metamorphic fluid is characterized by $a(H_2O)$ of 0.39–0.81 for the mineral assemblage in the inner rims of the garnets (high-pressure stage II) and high $a(H_2O)$ activities of 0.84–0.98 for the hydration stage of the eclogite-facies (high-pressure assemblage III) and the subsequent stages of decompression (blueschist- and greeschist-facies).

Keywords: Eo-Alpine high-pressure metamorphism, eclogites, *P-T-a(H₂O)* path, Sesia-Lanzo Zone, thermobarometry.

1. Introduction

High-pressure metamorphic belts play an important role in deciphering the evolution of collision orogens (e.g. MARUYAMA et al., 1996). Most of the information is gathered from relic mineral assemblages, which often represent a remnant of an earlier high-pressure/low temperature stage and are found as eclogites and blueschists (e.g. CARSWELL, 1990). The eclogites and exceptionally deep exposures of pre-Alpine continental crust in the Sesia-Lanzo Zone of northwestern Italy provide a window into the roots of a continent-continent collision orogenic system. Detailed examination of these lithologies yields significant constraints on the processes that lead to the formation of high-pressure rocks, which in turn is essential in deciphering the metamorphic history of collision orogens. Detailed petrographic examination and interpretation of petrological data from eclogites is hampered by several problems which are discussed below.

[1] Institut für Mineralogie und Petrographie, Universität Innsbruck, Innrain 52, A-6020 Innsbruck, Austria. <peter.tropper@uibk.ac.at>

[2] Department of Geological Sciences, University of Michigan, 2534 C.C. Little Building, Ann Arbor, MI 48109-1063, USA. <essene@umich.edu>

The role of fluids during high-pressure metamorphism, especially eclogite-facies metamorphism, has been the focus of intense research over many years (e.g. JAMTVEIT and YARDLEY, 1997). Eclogites were traditionally considered as rocks containing the anhydrous assemblage garnet + omphacite + rutile ± kyanite ± quartz, although OH-bearing minerals such as amphiboles, micas and clinozoisite/zoisite frequently occur (HAÜY, 1822). Full hydration of the basaltic precursor in the blueschist-facies consumes 5–6 wt% H_2O (PEACOCK, 1993), but there is also petrographic evidence that some pillow lavas and olivine gabbros of the Allalin gabbro complex in the Western Alps (BEARTH, 1967; CHINNER and DIXON, 1973), the Ötztal-Stubai crystalline complex (MILLER, 1974) and the Koralpe crystalline complex (MILLER and THÖNI, 1997) from the Eastern Alps, proceeded directly from anhydrous igneous precursors to eclogites. In contrast, the occurrence of hydrous minerals like amphibole, mica, clinozoisite/zoisite and the presence of fluid inclusions in the "anhydrous" mineral assemblage suggests that many eclogites equilibrated with a fluid phase at some point during their metamorphic history. There is macroscopic and microscopic evidence of the presence of a fluid phase in many blueschist- and eclogite-facies rocks: (1) The occurrence of veins with high-pressure mineral assemblages which suggests local $P_{Fluid} \geq P_{Total}$ (AUSTRHEIM, 1987; PHILIPPOT, 1987; BARNICOAT, 1988; HENRY et al., 1996), and (2) fluid inclusions, for example in Alpine high-pressure rocks suggest that the fluid might be saline and rich in trace elements such as Zr, Ti, REE (PHILIPPOT and SELVERSTONE, 1991; NADEAU et al., 1993; PHILIPPOT et al., 1995).

Although the metamorphic evolution of high-pressure rocks from the Sesia-Lanzo Zone has been the focus of several investigations (e.g. COMPAGNONI et al., 1977; POGNANTE, 1991; COMPAGNONI et al., 1993; VENTURINI, 1995), information about the metamorphic pore fluid interacting is scarce. For a full understanding, it is therefore important to relate the evidence of fluid-rock interaction with the observed pressure *(P)*-temperature *(T)* path of metamorphic rocks. The construction of a *P-T-a*(H_2O) path requires that the fluid history of a metamorphic cycle be correlated with the metamorphic crystallization sequence of characteristic mineral assemblages and hence to the pressures and temperatures imposed on it.

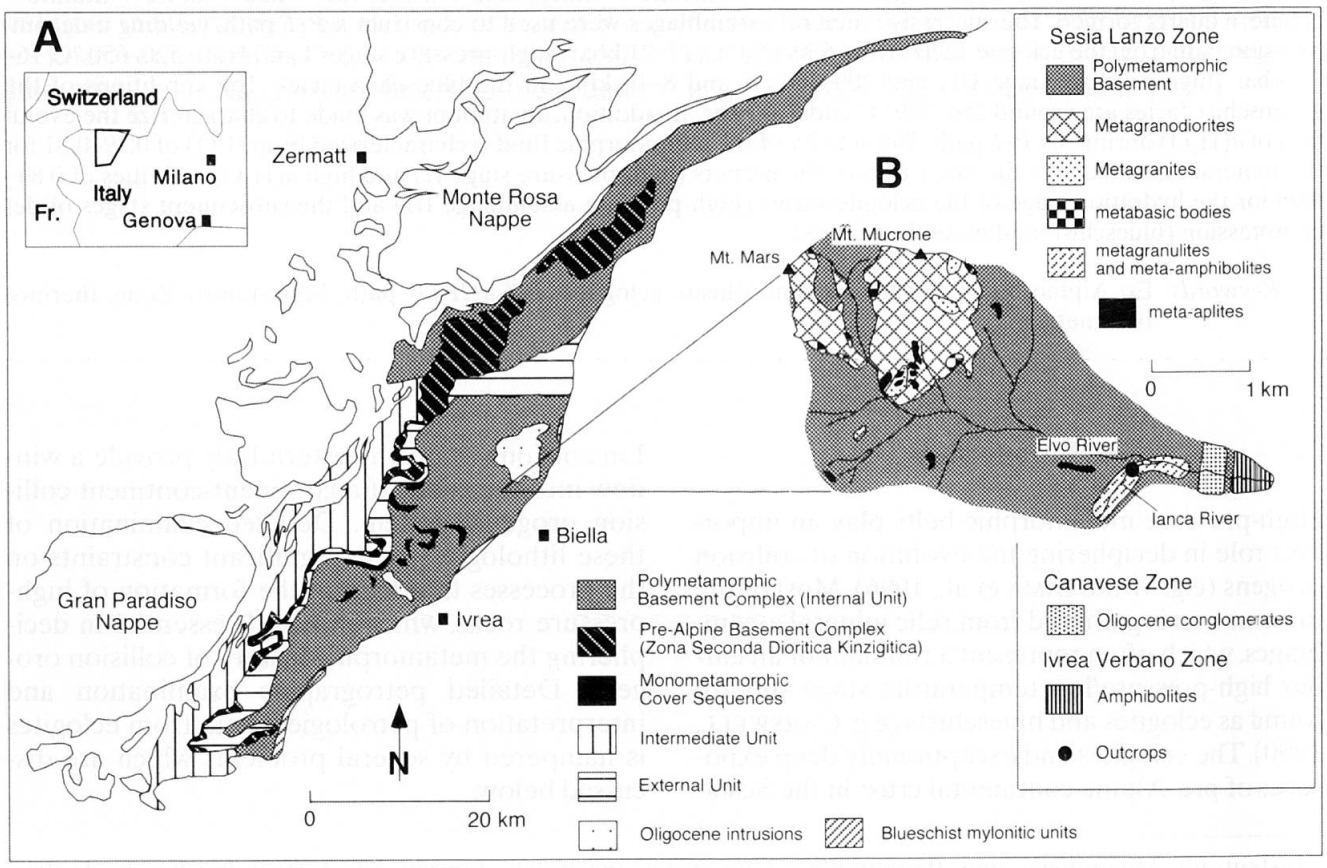

Fig. 1 (A) Geological overview over the Sesia-Lanzo Zone, Western Alps (Italy). (B) schematic overview over the outcrops at the Ianca river based on the map of ARMANDO (1992). The black circle indicates the locality of the outcrops at the Ianca river.

In this paper, the *P-T-a*(H_2O) path of complex eclogites in the Ianca Valley near Biella in Northern Italy from the Sesia-Lanzo Zone is constructed by combining textural relations and thermobarometric calculations. These eclogites were subjected to the Eo-Alpine high-pressure metamorphism and subsequently to retrogression under late-eclogite, blueschist- and greenschist-facies conditions. This leads to the formation of several mineral assemblages. In addition, the rocks show textural evidence of fluid-rock interaction under eclogite-facies conditions by the presence of (1) well preserved veins containing OH-bearing minerals in high-pressure mineral assemblages that crosscut the main foliation and (2) mineralogical evidence, such as leaching of elements along fractures. These features provide an opportunity to document fluid-rock interaction in eclogite-facies rocks, to determine the fluid composition from simplified phase equilibrium calculations with assemblages from different stages of the metamorphic evolution, and hence to derive a *P-T-a*(H_2O) path for these rocks.

2. Geological overview

The Sesia-Lanzo Zone is one of the internal Austroalpine units of the Western Alps in northern Italy (DAL PIAZ et al., 1972; COMPAGNONI et al., 1977) (Fig. 1A). Based on comprehensive petrographic and structural investigations, it is subdivided into three main complexes (VENTURINI et al., 1994; VENTURINI, 1995): (1) The Polymetamorphic Basement Complex, (2) the Monometamorphic Cover Sequences and (3) the Pre-Alpine Basement Complex ("Seconda Zona Dioritica Kinzigitica" or IIDK). The Polymetamorphic Basement Complex contains three units with different Alpine metamorphic characteristics (PASSCHIER et al., 1981). The Internal Unit, formerly known as the "Eclogitic Micaschist Unit" in the east, equilibrated under Eo-Alpine eclogite-facies conditions and shows subsequent blueschist-facies and only a minor greenschist-facies overprint. Towards the west, the Intermediate Unit, with an increasingly developed greenschist-facies overprint, is followed by the External Unit, which is almost completely overprinted by greenschist-facies assemblages. The latter two units are also known as the Gneiss Minuti Unit (COMPAGNONI et al., 1977). The Monometamorphic Cover Complex contains Triassic metabasalts and terrigenous sequences and crops out as a continuous belt in the central and southern Sesia Zone. The Pre-Alpine high-temperature Basement Complex ("Seconda Zona Dioritica Kinzigitica" or IIDK) is scattered throughout the Sesia-Lanzo Zone and contains Hercynian high-temperature basement rocks (DAL PIAZ et al., 1972). Recent geochronological investigations with robust systems, such as U–Pb on zircon and Sm/Nd and Lu/Hf dating of garnet, point to a Cretaceous/Tertiary age of 65–69 Ma for the high pressure metamorphism in the Sesia-Lanzo Zone (RUBATTO et al., 1999; DUCHÊNE et al., 1997). These ages are in contrast to earlier data that indicated an Early Cretaceous subduction of the Sesia-Lanzo Zone (HUNZIKER, 1974; OBERHÄNSLI et al., 1985; VENTURINI, 1995). Definite age constraints for the retrograde portion of the *P-T* path of the central Sesia-Lanzo Zone are scarce. Ar/Ar dating of glaucophanes, related to the subsequent blueschist-facies overprint, yielded erroneously old ages due to excess-Ar (VENTURINI, 1995) and geochronological investigations with Rb/Sr on white micas from the central Sesia-Lanzo Zone (eclogite micaschist unit) show evidence for partial resetting by an event younger than 55 Ma (INGER et al., 1996). In contrast to the central Sesia-Lanzo Zone, age data from the westernmost unit of the Sesia-Lanzo Zone (Gneis Minuti) which underwent pervasive greenschist-facies metamorphism, give ages of 38–39 Ma (INGER et al., 1996). The samples under investigation are eclogites, which were collected along a ca. 400 m long section along the Ianca River near the village of Graglia, 10 km west of Biella. These outcrops occur in the easternmost part of the Polymetamorphic Basement Unit near the Canavese Zone, as shown in the interpretative geological inset map in Fig. 1B, which is based on field work by ARMANDO (1992).

3. Field relations

Eclogites: Most of the eclogites are coarse-grained and show varying degrees of foliation, depending on the intensity of blueschist-facies mylonitization. Some outcrops show interlayering of dark omphacite + garnet + amphibole layers and light clinozoisite ± zoisite + paragonite layers. The main foliation contains the assemblage garnet + omphacite + clinozoisite/zoisite + amphibole and dips to the NW. Crosscutting veins occur isolated in coarse grained rocks over a very restricted small area of about 100 m in length. Later shearing has led to the formation of at least two glaucophane-bearing mylonitic foliations dipping SE and NW. Massive amphibole-rich layers intercalated with the eclogites show almost no foliation and contain very coarse grained amphiboles (3–5 cm wide layers). Some of these layers show compositional layering, where the dark layers are now

composed of hornblende and the light layers contain clinozoisite, zoisite and chlorite.

Veins: The veins crosscut the main foliation and in many cases form sharp contacts with the host rock. Most veins represent single fractures, but some veins show a network of fractures, where small fractures radiate outward from a larger fracture (Fig. 2). Late-stage blueschist-facies shear zones (cm-wide) have deformed some of the veins. The veins usually contain laarge, dark amphibole porphyroblasts in a white maatrix composed of the assemblage clinozoisite + zoisite

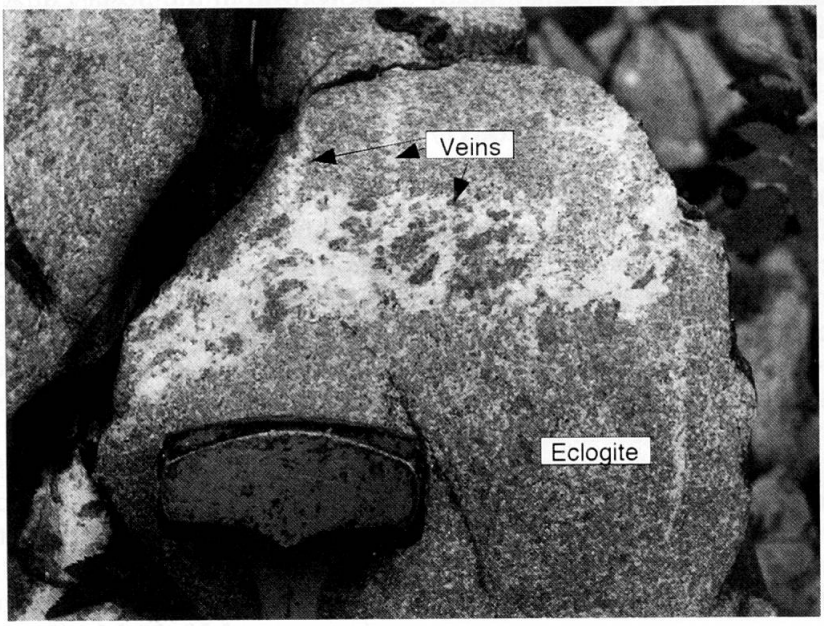

Fig. 2 Photograph of a barroisite + paragonite + clinozoisite/zoisite + quartz ± omphacite bearing vein from pooorly foliated eclogite.

	High pressure stage I Grt core Inclusions	High pressure stage II Grt rim Inclusions	High pressure stage III Grt outer rim Inclusions	High pressure stage III Matrix	High pressure stage III Veins	Blueschist facies Matrix	Greenscchist faciess Matrixx
Garnet	----------	----------	----------	----------			
Omphacite		----------	----------	----------	--------?--------		
Kyanite	----------	----------					
Paragonite	----------		----------	----------	----------		
Clinozoisite	----------	----------	----------	----------	----------	----------	----------
Zoisite	----------	----------	----------	----------	----------	--------?--------	
Rutile	----------	----------	----------	----------	----------	----------	
Barroisite			----------	----------	----------		
Glaucophane						----------	
Actinolite							----------
Dolomite			----------	----------	----------	--------?--------	
Zircon			----------	----------			
Chlorite							----------
Muscovite				----------			----------
Talc							----------
Albite							----------
Titanite							----------
Calcite							----------
Quartz	----------	----------	----------	----------	----------	----------	----------

Fig. 3 Mineral assemblages from eclogites and their relation to the different stages of the observed *P-T* path.

+ paragonite + quartz ± omphacite. Parts of the relic host rock assemblage, like fractured garnet and omphacite porphyroblasts, can still be found in the veins as aggregates, or single crystals encapsulated in the white matrix.

4. Textural relations and petrography

The mafic rocks in the Ianca Valley were fully equilibrated under Eo-Alpine metamorphic conditions (ARMANDO, 1992). The rocks show extensive overprintings which led to the formation of different assemblages in the eclogite-, and subsequent blueschist- and greenschist-facies. In order to reconstruct the metamorphic history, one must distinguish between mineral assemblages present as inclusions in garnet porphyroblasts and those in the matrix. The sequence of mineral assemblages is shown in Figure 3.

4.1. ECLOGITES

4.1.1. Inclusion assemblages

Most are found in garnet porphyroblasts as small inclusions (5–20 μm in diameter) and their modal amounts are quite variable (Fig. 4A). Based on the disappearance of paragonite during garnet growth, it is possible to distinguish between three sequential inclusion assemblages in the cores and the rims of the garnets.

Garnet core inclusion assemblage (high-pressure assemblage I): In the cores of few garnets, the inclusion assemblage paragonite + kyanite + quartz + clinozoisite ± zoisite is observed (Fig. 4B). In one sample (IBSF 71), the assemblage paragonite + kyanite + clinozoisite + muscovite was also found in an omphacite (Fig. 4C). The amount of clinozoisite included in garnet varies greatly. Occasionally, inclusion-rich zones surround an inclusion-free garnet core, and zones consisting only of clinozoisite inclusions can be found.

Inner garnet rim inclusion assemblage (high-pressure assemblage II): Towards the outer parts of the garnets, paragonite disappears and the assemblage omphacite + clinozoisite + kyanite + quartz + rutile ± zoisite appears. Matrix omphacite porphyroblasts contain in some instances kyanite, dolomite, clinozoisite or quartz inclusions. Kyanite occurs in all host minerals as very small needles (5–10 μm); its identification was confirmed with micro-Raman spectroscopy (Rainhard Kaindl, pers. comm.). Rutile inclusions also occur in the garnet rims. In many cases, these rutiles can be quite large (<100 μm) and contain themselves dolomite inlcusions and occasionally omphacite + dolomite inclusions. The assemblage garnet + omphacite + kyanite + clinozoisite + rutile + quartz ± dolomite close to the outermost rims of the garnet is regarded as the eclogite-facies peak metamorphic assemblage (Fig. 4D).

Outer garnet rim inclusion (high-pressure assemblage III): In a few samples (IBSF 58VI, IBSF 61VI), some garnet porphyroblasts show another inclusion-rich zone external to the peak eclogite-facies peak inclusion assemblage (Fig. 4E). These garnets contain the inclusion assemblage omphacite ± barroisite + rutile + quartz + zircon.

4.1.2. Matrix assemblages

The most important feature of the matrix assemblages is the absence of kyanite. The matrix in the eclogites is strongly overprinted by hydrated assemblages of subsequent eclogite-, blueschist- and greenschist-facies metamorphism and contains therefore several different mineral assemblages.

Eclogite-facies assemblage (high-pressure assemblage III): This assemblage is composed of garnet + omphacite + barroisite + clinozoisite + quartz + rutile + paragonite ± muscovite ± dolomite, but without kyanite. This assemblage correlates with the high-pressure assemblage III from the garnet inclusion assemblages. The abundance of H_2O-bearing minerals and abundant fluid inclusions in the cores of some matrix amphiboles, in omphacites and in garnet rims suggests that these minerals equilibrated with a fluid at this stage. Garnet continued to grow next to the amphibole porphyroblasts and also along trails parallel to the cleavage planes in the amphiboles. In sample IBSF 58 VI, garnet grew along veins (Fig. 4F). The assemblage clinozoisite + rutile + dolomite + zircon grew along trails within the amphibole. Omphacites also show abundant dolomite and rutile inclusions (Fig. 4G). REE-bearing epidote cores are found in clinozoisite inclusions in barroisite (Fig. 4H). The assemblage dolomite + rutile is also very common and forms trails within the barroisite porphyroblasts (Fig. 4I). The barroisites also show some irregular zoning in their cores, indicating fracturing and leaching along the fractures (Fig. 4J).

Blueschist-facies assemblage: Glaucophane appears at this stage. Textural evidence suggests that omphacite is not stable, since it is rimmed by glaucophane, indicating a possible replacement reaction. Glaucophane usually grows around barroisite (Fig. 4J) and, in one sample (IBSF 12), also overgrows paragonite.

Greenschist-facies assemblage: The texturally latest mineral parageneses is represented by the assemblage actinolite + chlorite + muscovite + albite + calcite + talc + titanite + clinozoisite. Phengitic muscovite overgrows paragonite, and they form complex intergrowths where paragonite is replaced across its grain boundaries (Fig. 4K). Barroisite shows replacement by the assemblage chlorite + actinolite + albite during greenschist-facies overprint (Fig. 4 M), whereas omphacite is replaced by actinolite + albite (Fig. 4N) and glaucophane is replaced by actinolite + albite + chlorite. Titanite forms thin rims aroound rutile grains.

4.2. AMPHIBOLITES

The massive amphibolites comprise the assemblage hornblende + clinozoisite + zoisite + chlorite ± paragonite ± garnet. Amphiboles appear slightly zoned and form large porphyroblasts that show inclusions of rutile and clinozoisite with REE-rich cores and occasionally small garnet inclusions. Garnet porphyroblasts in sample IBSF 17 conntain

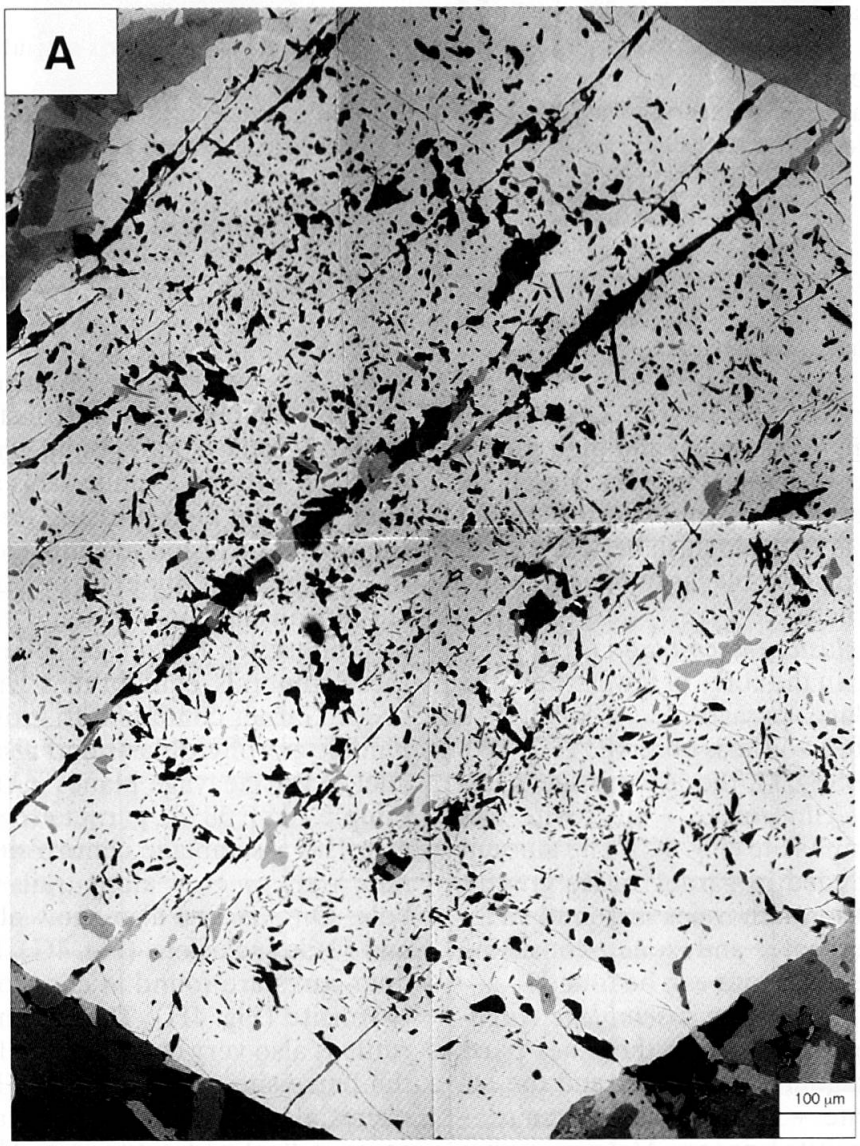

Fig. 4 Backscattered electron (BSE) images of the most important textural features:
(A) Overview over an inclusion-rich garnet porphyroblast (IBSF 71). **(B)** Early prograde inclusion assemblage inn the core of a garnet (Grt) porphyroblast (sample IBSF 71); the assemblage comprises paragonite (Pg) + clinozooisite (Czo) + zoisite (Zo) + kyanite (Ky) + quartz (Qtz). Some inclusions were affected by later retrogression along ssmall fractures, resulting in the replacement of paragonite by muscovite or albite. **(C)** Pg + Ky + Czo + Zo + muscovite ((Ms) inclusions in an omphacite (Omp) crystal, sample IBSF 71. The surrounding matrix consists of Pg. **(D)** Peak eclogite-facies inclusion assemblage Omp + Czo + Ky + Qtz in a garnet rim (sample IBSF 22A). **(E)** Outermost garnett rim with Omp and rutile (Rt) inclusions (sample IBSF 61VI). Grt core on the upper right side includes the high-presssure peak assemblage Omp + Ky + Qtz.

the inclusion assemblage zoisite + kyanite + rutile + phengite + quartz. Former igneous amphiboles still retain their shape but are completely pseudomorphed by the greenschist-facies assemblage albite + chlorite + clinozoisite + titanite. Actinolite and titanite formed along small fractures within

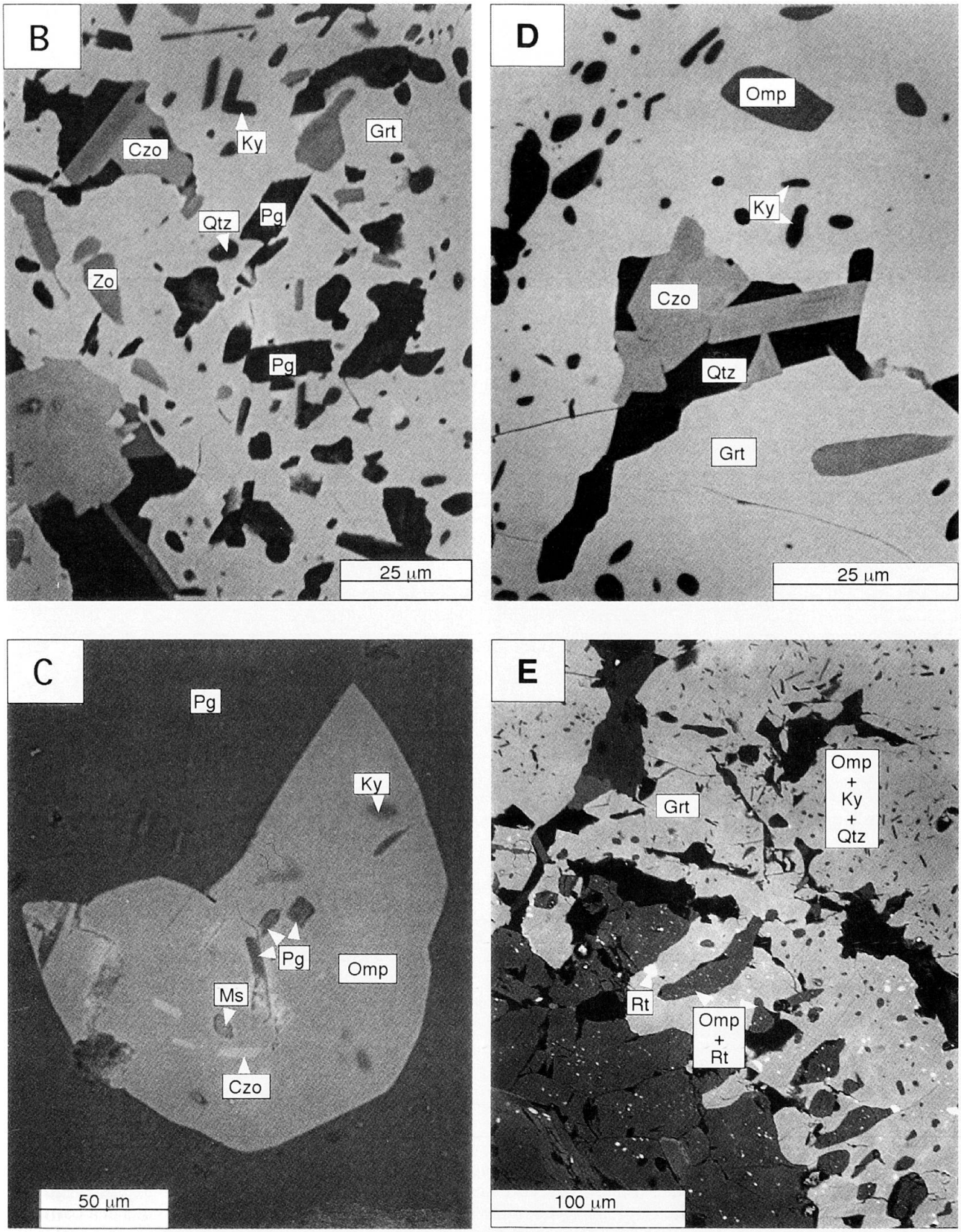

Fig. 4 (continued)

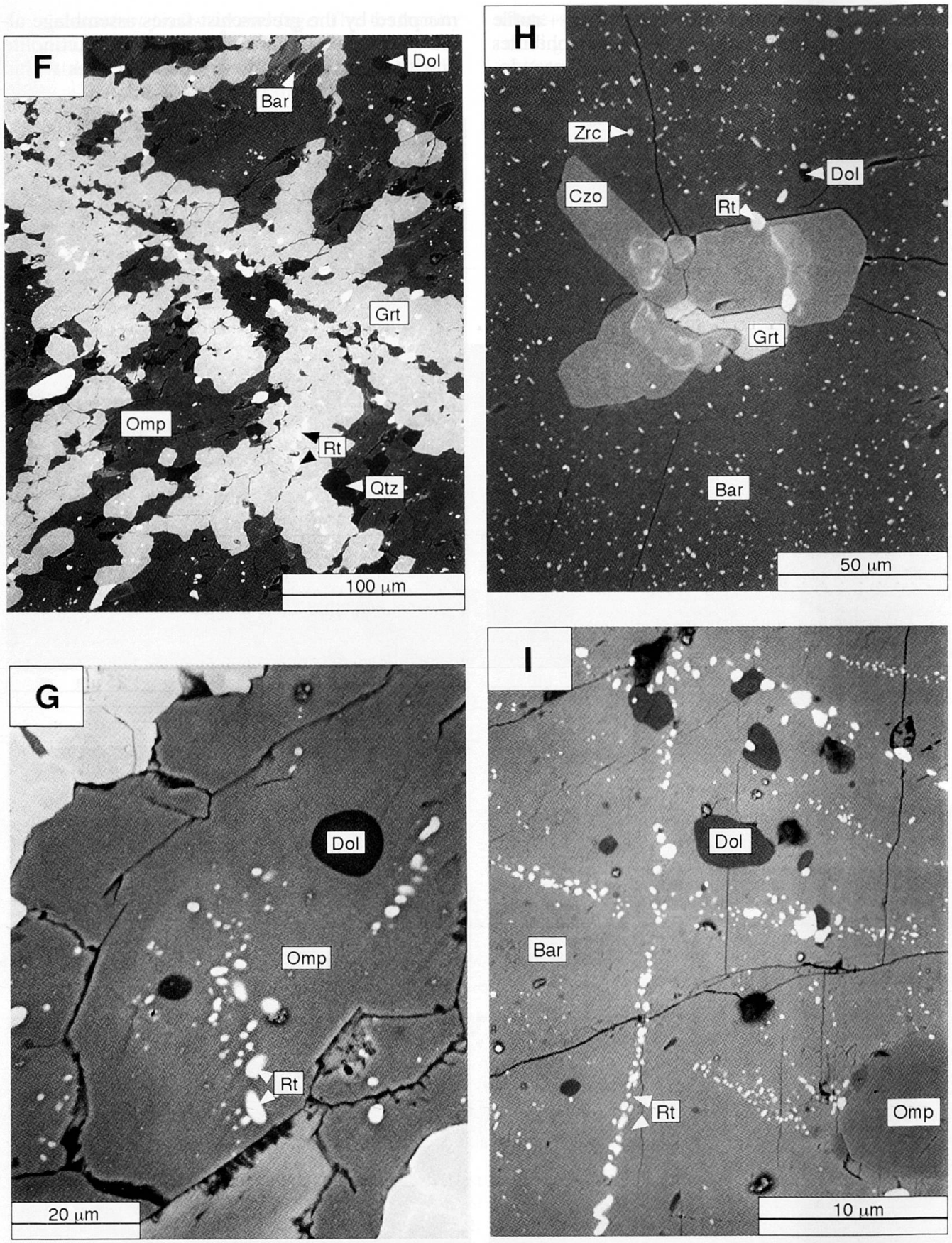

Fig. 4 (cont.) **(F)** Garnet vein in an Omp + barroisite (Bar) aggregate (sample IBSF 58 VI). The vein consists of Grt, Qtz and Rt. Note that omphacite also occurs in the core of the vein. **(G)** Omp from omphacite + barroisite aggregate with inclusions of ferroan dolomite (Dol) and Rt, sample IBSF 58 VI. **(H)** Czo + Grt + Rt inclusions in a barroisite porphyroblast. Clinozoisite shows clouded REE-bearing cores; barroisite contains Dol, Rt and zircon (Zrc) inclusions, sample IBSF 4. **(I)** Trails of dolomite and rutile in barroisite porphyroblast (IBSF 10). **(J)** Amphibole zoning

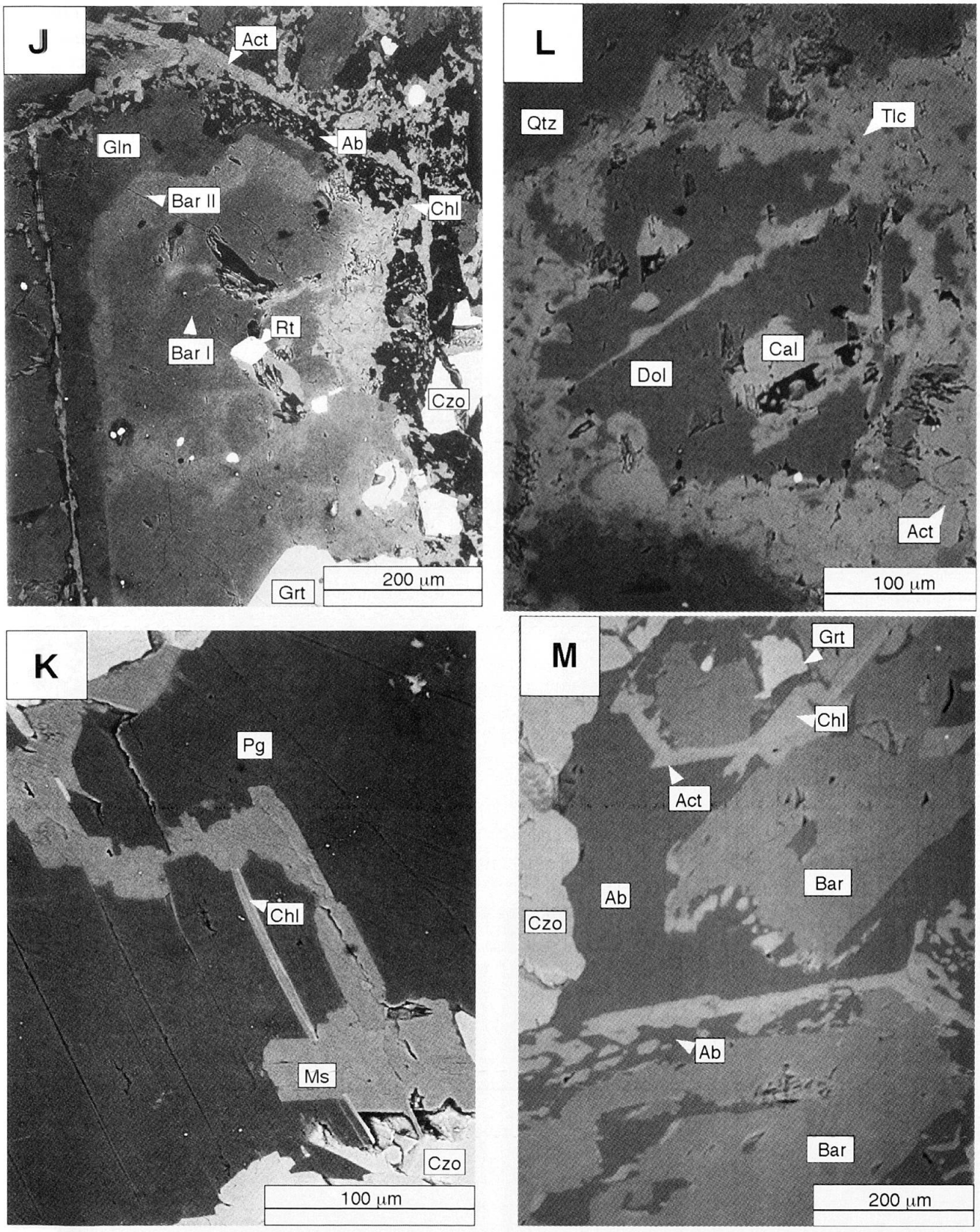

with barroisite core (Bar I: dark; Bar II: light), glaucophane (Gln) mantle and actinolite (Act) outermost rim (sample IBSF 10). Note zonation in barroisite core, ranging from Fe^{2+}-poor to Fe^{2+}-rich barroisite compositions towards the rim of the core. Core (Bar I) contains Rt inclusions; healed fractures in the core correspond to Fe^{2+}-rich barroisite (Bar II) composition. Actinolite in outermost rims is usually associated with albite (Ab) and chlorite (Chl). **(K)** Ms + Pg intergrowths, sample IBSF 10. Muscovite replaces paragonite across grain boundaries and contains few chlorite (Chl) lamellae. **(L)** Dol porphyroblast in high-pressure vein replaced by calcite (Cal) + talc (Tlc) + Act, sample IBSF 22A. Surrounding matrix consists of Qtz. **(M)** Replacement of barroisite (Bar) by actinolite (Act) + albite (Ab) + chlorite (Chl).

the amphibole porphyroblasts during retrogression. Small amphibolite layers or segregations that are interlayered with the eclogites are made of the assemblage garnet + hornblende + clinozoisite. Garnet in these layers shows abundant amphibole and clinozoisite inclusions (Fig. 4O). These garnets also preserve relics of old garnet cores, which appear faint in electron backscatter (BSE) images.

4.3. VEINS

Veins crosscutting the eclogites are characterized by the assemblage barroisite + paragonite + clinozoisite + zoisite + quartz ± omphacite (Fig. 4P) and correspond to the latest eclogite-facies stage of the host rocks. Barroisite occasionally contains omphacite inclusions and forms dark-green patches of up to 3 cm in diameter. The eclogite-facies peak assemblage consisting of relict garnet porphyroblasts with kyanite inclusions can be found within the veins. In one sample (IBSF 22A), large aggregates (0.5–2 cm) of dolomite + quartz are rimmed by barroisite porphyroblasts. The dolomite is in most cases completely replaced by the

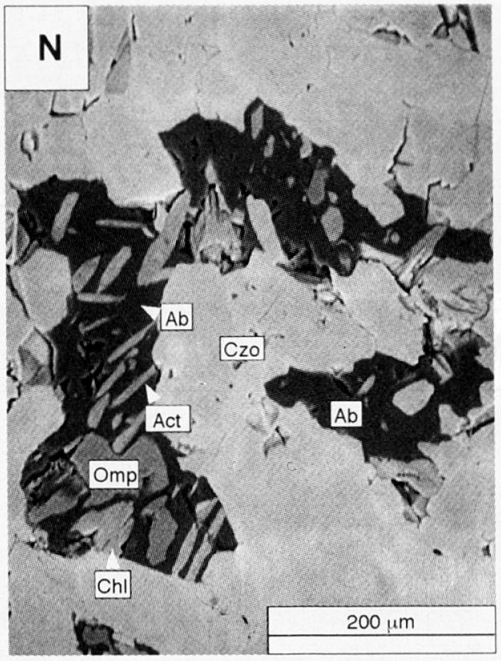

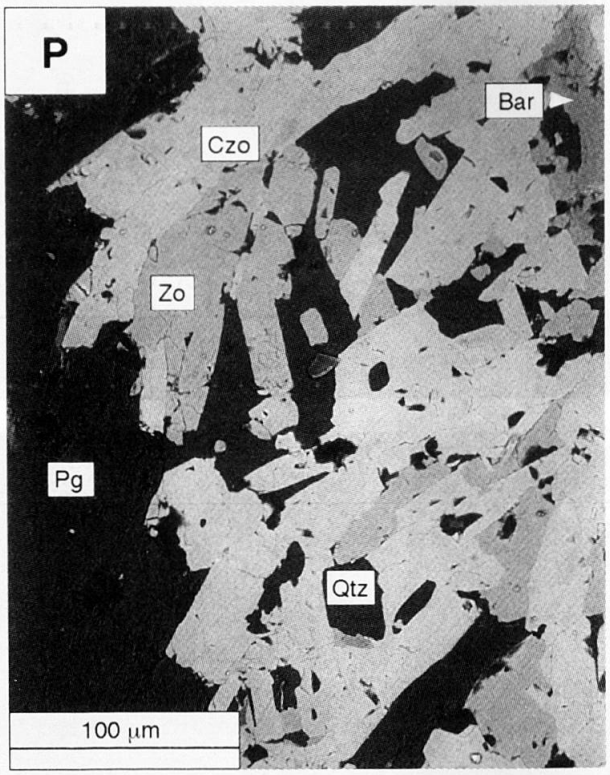

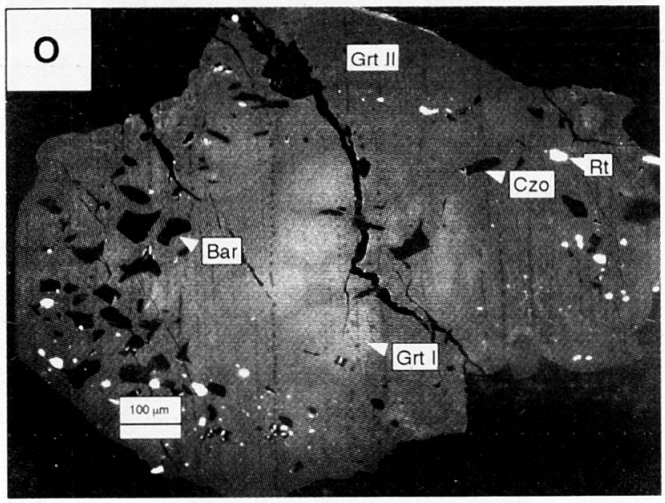

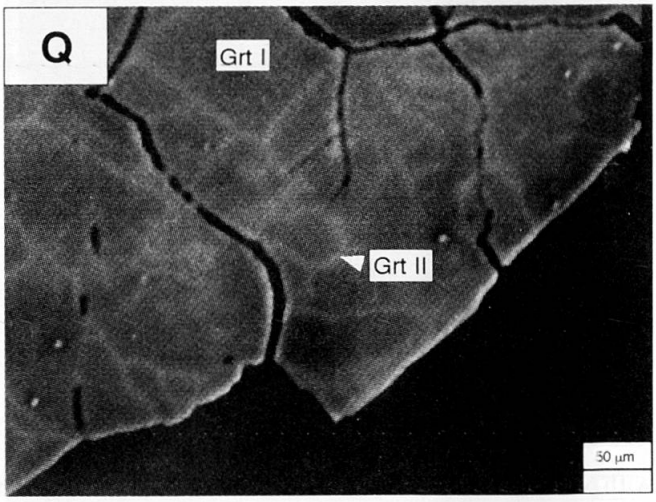

Fig. 4 (cont.) **(N)** Replacement of omphacite (Omp) by actinolite (Act) + albite (Ab) + chlorite (Chl). **(O)** Garnet porphyroblast in amphibolite layer. Garnet shows faint relics of an earlier garnet (Grt I) in the core. **(P)** Mineral assemblage in high-pressure vein from sample IBSF 22A. Assemblage contains Pg + Czo + Zo + Bar + Qtz. **(Q)** Healed fractures at rim of garnet porphyroblast (Grt I), sample IBSF 22A. Garnet along these fractures is slightly more Fe^{2+}-rich (Grt II). Mineral abbreviations are according to KRETZ (1983).

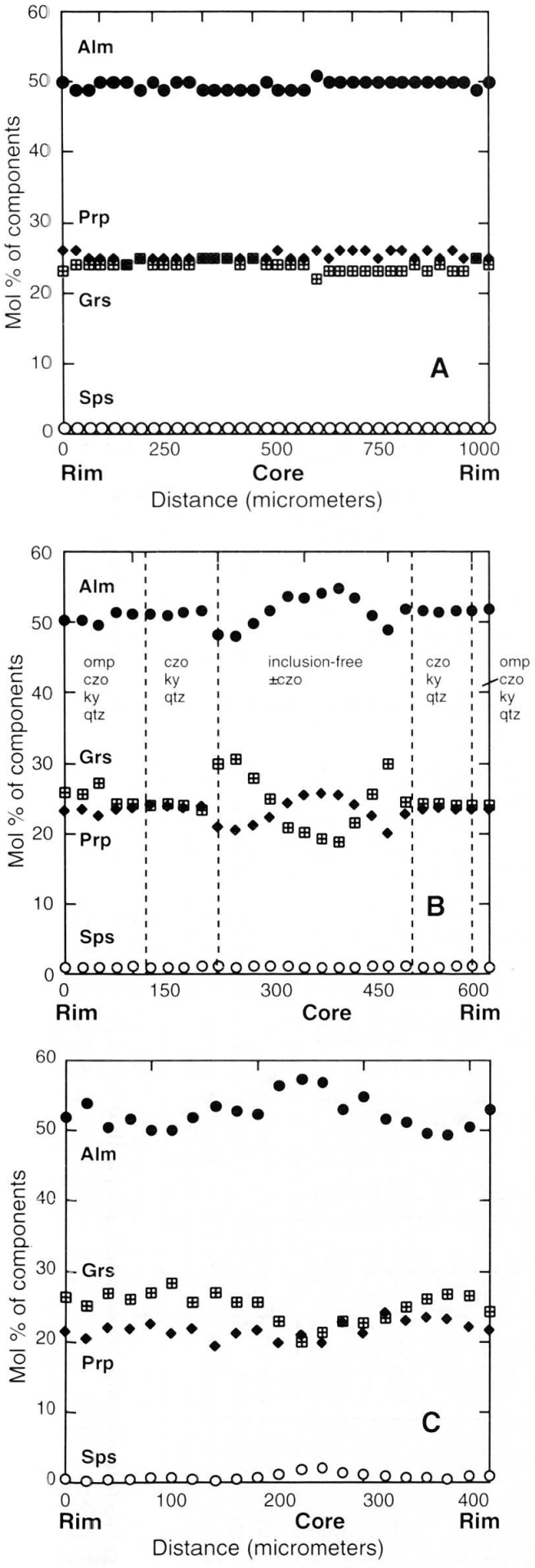

assemblage calcite + actinolite + talc (Fig. 4L). The amphiboles in these porphyroblasts exhibit the same chemical zonation as the amphiboles in the host rocks with cores of barroisite, glaucophane rims and outermost rims of actinolitic hornblende. In contrast to the amphiboles in the host rock, which show many inclusions (zircon, rutile, allanite), those in the veins contain almost no inclusions. Large paragonite porphyroblasts overgrew relict assemblages and clinozoisite + paragonite frequently replace omphacite porphyroblasts.

5. Mineral chemistry

Garnet: The analyses are shown in Table 1 and the analytical conditions are in Appendix 1. All garnets show extensive fracturing with the formation of a fine network of cracks throughout the porphyroblasts (Fig. 4Q). The garnet composition changes along these cracks from Alm_{55} to Alm_{65}. Most garnets show no compositional zoning (Fig. 5A). Prograde compositional zoning, was observed in only two samples (IBSF 7, IBSF 19) (Fig. 5B). These garnets show an increase in grossular content in the core from Grs_{18} to Grs_{31}. In the rim, the grossular content decreases again down to Grs_{25}. Not all garnets show an increase in grossular component towards the rims. Sample IBSF 40 shows a Ca plateau in the core (Grs_{29}) and a sudden decrease of Ca towards the rim (Grs_{18}) as the pyrope content increases slightly. Some garnets show an outermost rim, containing the inclusion assemblage barroisite + omphacite + rutile, which grew during the hydration stage of the eclogite-facies (high-pressure assemblage III). In these rims, the grossular content drops slightly from approximately 24 to 21 mol%. Garnets growing along the cleavage of barroisite porphyroblasts also show a similar decline in the grossular content. The garnets in the amphibolite layers (sample IBSF 34) retain a prograde zoning with an increase in grossular and pyrope from the core (Grs_{19}, Prp_{18}) to the rim (Grs_{26}, Prp_{23}, Fig. 5C). The pyrope content decreases slightly at the rim and along fractures within the garnet from Prp_{23} to Prp_{21}, owing to later retrogression. In amphibolite sample IBSF 34, an old garnet core, which can

Fig. 5 (A) Compositional zoning profile across garnet porphyroblast from eclogite (sample IBSF 19B). (B) Correlation between compositional zoning and inclusion assemblages in garnet porphyroblast from eclogite sample IBSF 19B. (C) Compositional zoning across garnet crystal from amphibolitic layer. Alm: almandine, Grs: grossular, Prp: pyrope, Sps: spessartine.

Table 1 Representative electron microprobe analyses of garnet*.

	1 core	2 rim	3 relict	4 core	5 mantle	6 rim	7 core	8 mantle	9 rim	10 core	11 core	12 rim	13 fracture	14 core	15 rim	16 core	17 vein	18 vein
SiO_2	39.28	38.42	38.35	38.77	38.80	39.45	38.20	38.52	38.60	39.06	38.81	39.42	38.12	39.26	39.57	39.01	38.92	38.97
TiO_2	0.05	0.04	0.09	0.03	0.04	0.03	0.46	0.49	0.03	0.07	0.10	0.02	0.08	0.08	0.05	0.06	0.22	0.16
Al_2O_3	21.05	21.21	21.02	21.42	21.24	22.05	20.78	20.90	21.36	22.31	21.76	22.15	21.61	21.87	22.11	22.01	21.54	21.64
Cr_2O_3	0.09	0.06	0.10	n.d.	n.d.	n.d.	n.d.	0.02	n.d.	n.d.	n.d.	n.d.	n.d.	0.02	0.02	n.d.	n.d.	0.04
FeO	24.17	25.89	27.01	23.82	23.43	22.05	25.68	25.33	25.42	23.89	24.65	22.99	28.21	23.75	21.90	23.66	23.91	24.24
MnO	0.20	0.88	0.99	0.46	0.39	0.40	0.94	0.70	0.77	0.50	0.56	0.44	0.99	0.76	0.58	0.50	0.58	0.54
MgO	5.57	5.04	4.58	5.85	4.59	6.44	3.58	3.64	4.46	6.63	6.37	7.06	5.47	7.16	7.55	6.61	6.33	6.57
CaO	9.64	7.65	7.05	9.44	11.19	8.53	9.87	10.38	8.83	8.10	7.48	7.86	5.25	7.49	8.44	8.44	7.94	8.12
Σ	100.05	99.19	99.20	99.77	99.67	100.32	99.52	99.98	99.46	100.56	99.74	99.95	99.73	100.39	100.22	100.29	99.44	100.28
Si	3.04	3.02	3.03	3.01	3.02	3.02	3.02	3.02	3.03	2.99	3.01	3.02	2.99	3.01	3.02	3.00	3.02	3.00
Al	1.92	1.97	1.96	1.96	1.95	1.99	1.93	1.93	1.97	2.01	1.99	2.00	2.00	1.98	1.99	1.99	1.97	1.97
Ti	<0.01	<0.01	0.01	<0.01	<0.01	<0.01	0.03	0.03	<0.01	<0.01	0.01	<0.01	<0.01	<0.01	<0.01	<0.01	0.01	0.01
Cr	0.01	<0.01	0.01	n.d.	n.d.	n.d.	n.d.	n.d.	n.d.	n.d.	n.d.	n.d.	n.d.	<0.01	<0.01	n.d.	n.d.	<0.01
Fe^{2+}	1.57	1.70	1.78	1.55	1.53	1.50	1.70	1.66	1.67	1.53	1.60	1.47	1.85	1.52	1.40	1.52	1.55	1.56
Mn	0.01	0.06	0.07	0.03	0.03	0.03	0.06	0.05	0.05	0.03	0.04	0.03	0.07	0.05	0.04	0.03	0.04	0.04
Mg	0.64	0.59	0.54	0.68	0.53	0.74	0.42	0.42	0.52	0.76	0.74	0.81	0.64	0.82	0.86	0.76	0.73	0.76
Ca	0.80	0.64	0.60	0.78	0.93	0.70	0.83	0.87	0.74	0.66	0.62	0.65	0.44	0.61	0.69	0.70	0.66	0.67
Σ	7.99	7.98	8.00	8.01	7.99	7.98	7.99	7.98	7.98	7.98	8.01	7.99	8.00	8.01	8.02	8.01	7.98	8.01
Alm	0.52	0.57	0.60	0.51	0.51	0.51	0.56	0.55	0.56	0.51	0.53	0.50	0.62	0.51	0.47	0.51	0.52	0.52
Prp	0.22	0.20	0.18	0.22	0.18	0.25	0.14	0.14	0.17	0.26	0.25	0.27	0.22	0.27	0.29	0.25	0.25	0.25
Grs	0.26	0.21	0.20	0.26	0.31	0.24	0.28	0.29	0.25	0.22	0.21	0.22	0.15	0.20	0.23	0.23	0.22	0.22
Sps	<0.01	0.02	0.02	0.01	<0.01	<0.01	0.02	0.02	0.02	0.01	0.01	0.01	0.01	0.02	0.01	0.01	0.01	0.01

*Formulae normalized to 12 oxygens; n.d.—not detected.

Alm: [Fe/(Fe+Mg+Ca+Mn)], Prp: [Mg/(Fe+Mg+Ca+Mn)], Grs: [Ca/(Fe+Mg+Ca+Mn)], Sps; [Mn/(Fe+Mg+Ca+Mn)].

[1] garnet rim, [2] garnet core and [3] relict garnet in core, sample IBSF 34; [4] Garnet core without inclusions, [5] garnet from czo-rich inclusion zone, [6] garnet rim with omp + ky + czo + qtz inclusions, sample IBSF 19B; [7] inclusion-free garnet core, [8] garnet from czo + qtz inclusion zone and [9] garnet rim, sample IBSF 40; [10] core of homogenous garnet, sample IBSF 10; [11] garnet core and [12] garnet rim, sample IBSF 22A (Grt I of Fig. 4Q) ; [13] garnet composition along a fracture, sample IBSF 22A (Grt II of Fig. 4Q); [14] garnet core, [15] garnet rim of garnet from amphibolite, sample IBSF 17; [16] garnet core with omp + ky + czo + qtz inclusions, [17] garnet rim with omp + rt inclusions, sample IBSF 61 VI; [18] garnet from grt + rt + zirc vein in omp + bar aggregate, sample IBSF 58 VI.

only be seen as faint relic patches in BSE photographs, is preserved (Fig. 4O). Its composition, $Alm_{49-58}Prp_{20-27}Grs_{17-26}Sps_{0.5-1.5}$, is only slightly different than that of the rim.

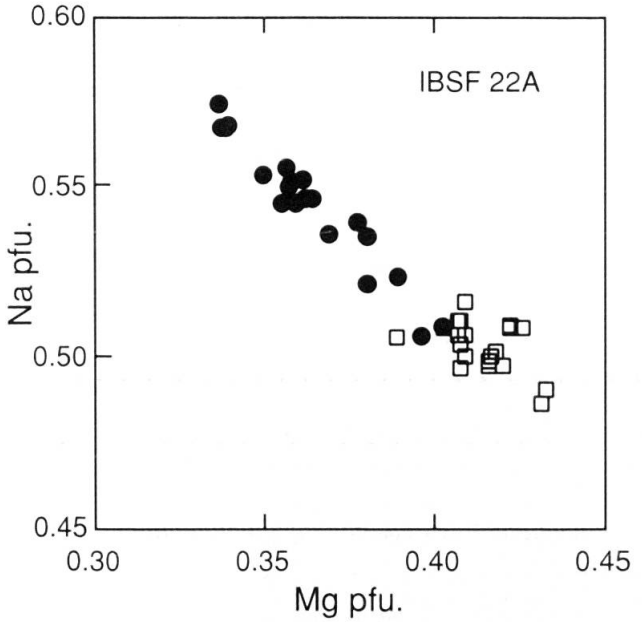

Fig. 6 Plot of Na apfu versus Mg apfu of matrix omphacites (open squares) and omphacite inclusions in garnet (filled circles) from sample IBSF 22A.

Clinopyroxene: All analyzed clinopyroxenes (Table 2) are omphacite. The matrix clinopyroxenes are homogeneous and frequently exhibit only a very slight irregular zoning with changes of only a few mol% of jadeite component. Omphacite inclusions in garnet have slightly higher Na pfu and lower Mg pfu (Fig. 6) and hence a slightly higher jadeite content (Jd_{47-52}), than matrix omphacites (Jd_{44-47}).

Amphibole: The amphiboles in the eclogites show a complex compositional zoning pattern. Optically, they show light blue cores and slightly blue-green rims. The cores are very often inclusion-rich. According to the nomenclature of LEAKE et al. (1997) the amphiboles have barroisite cores with inner rims of glaucophane and outermost rims of actinolite (Table 3; Fig. 7). They also show complex zoning in terms of the Fe^{2+}/Mg ratio within the cores. Ferroan barroisite grew along healed fractures across the cores and at the rims of the barroisite cores. Barroisite cores change slightly from inner to outer core with an increase in Fe^{2+} and a slight decrease in Na and Al (Table 3). The barroisites

Table 2 Representative electron microprobe analyses of pyroxene*.

	1 Incl.	2 Incl.	3 Matrix	4 Matrix	5 Incl.	6 Matrix	7 Incl.	8 Matrix	9 Matrix
SiO_2	55.53	55.87	56.00	55.78	55.53	56.12	56.08	55.55	55.88
TiO_2	0.07	0.06	0.05	0.03	0.19	0.06	0.06	0.06	0.19
Al_2O_3	12.59	12.58	11.49	11.72	12.47	11.00	12.31	11.31	11.13
Cr_2O_3	n.d.	n.d.	0.03	0.02	0.04	0.11	0.02	0.02	0.11
Fe_2O_3**	1.78	2.60	1.30	0.37	3.13	2.36	2.61	2.62	2.23
FeO	3.84	2.73	3.22	3.99	3.66	2.38	3.11	2.06	2.91
MnO	0.03	0.03	n.d.	0.05	n.d.	0.03	0.06	n.d.	n.d.
MgO	6.57	6.99	8.07	7.94	6.44	7.97	6.96	8.12	8.21
CaO	10.91	11.59	12.89	12.73	11.04	13.00	11.81	12.79	12.97
Na_2O	7.96	7.94	7.09	6.95	8.04	7.31	7.85	7.24	7.08
Σ	99.31	100.40	100.16	99.60	100.54	100.34	100.87	99.77	100.72
Si	1.98	1.97	1.98	1.99	1.97	1.99	1.98	1.98	1.98
$Al^{(IV)}$	0.02	0.03	0.02	0.01	0.03	0.01	0.02	0.02	0.02
$Al^{(VI)}$	0.52	0.50	0.46	0.48	0.49	0.45	0.49	0.45	0.44
Ti	<0.01	<0.01	<0.01	<0.01	0.01	0.01	<0.01	<0.01	0.01
Fe^{3+}	0.05	0.07	0.04	0.01	0.08	0.06	0.07	0.07	0.06
Fe^{2+}	0.12	0.08	0.10	0.12	0.11	0.07	0.09	0.06	0.09
Cr	n.d.	n.d.	<0.01	<0.01	<0.01	<0.01	<0.01	<0.01	<0.01
Mn	<0.01	<0.01	n.d.	<0.01	n.d.	<0.01	<0.01	n.d.	n.d.
Mg	0.35	0.37	0.43	0.42	0.34	0.42	0.37	0.43	0.43
Ca	0.42	0.44	0.49	0.49	0.42	0.49	0.45	0.49	0.49
Na	0.55	0.54	0.49	0.48	0.55	0.50	0.54	0.50	0.49

*Formulae normalized to 4 cations and 6 oxygens; **—calculated; n.d. —not detected; Incl.— inclusion.
[1, 2] omphacite inclusions in garnet and [3, 4] matrix omphacite coexisting with garnet, sample IBSF 22A; [5] omphacite inclusion in garnet; [6] matrix omphacite coexisting with garnet, sample IBSF 19B, [7] omphacite inclusion in garnet; [8] matrix omphacite coexisting with garnet, sample IBSF 7; [9] omphacite overgrown by vein-like garnet, sample IBSF 58VI.

plot very close to the end-member composition in the Na^{M4}–Al^{VI} diagram between tremolite/actinolite and glaucophane, but show considerable substitution on the A-site, indicating a solid solution towards edenite. Glaucophane forms rims around barroisite and also exhibits a slight increase of Ca and Fe towards the rim (Table 3). The outermost rims are composed of actinolite. The amphiboles in the amphibole-rich body are large bluish porphyroblasts of barroisite with inclusion-rich cores and clear rims (Table 3). Their compositions show considerable variation in Na on the A and M(4) sites, from 0.05 to 0.65 apfu on the A-site and 0.44 to 0.73 apfu on the M(4) site.

Clinozoisite and zoisite: Both minerals occur in the eclogite-facies veins, as well as in the matrix of the host rocks. The pistacite content [Ps = $100 \cdot Fe^{3+}/(Fe^{3+} + Al)$] of matrix clinozoisites and zoisites from texturally earlier stages (eclogite- and blueschist-facies) ranges from 12 to 17 and 5 to 7 mol% respectively (Table 4). In greenschist-facies assemblages, pistacite contents increase to ca. 20 mol%. In sample IBSF 19B, pistacite contents of clinozoisite vary from 11 to 13 mol%, whereas they range from 13 to 19 mol% where epidote is associated with the assemblage garnet + kyanite + quartz ± omphacite. In the less inclusion-rich rims, the pistacite contents drop back to

Table 3 Representative electron microprobe analyses of amphibole*.

	1 Barr.	2 Barr.	3 Barr.	4 Barr.	5 Gln.	6 Gln.	7 Act.	8 Act.	9 Barr.	10 Barr.
SiO_2	51.98	52.43	51.61	51.42	58.36	56.87	56.48	56.36	48.61	50.19
TiO_2	0.12	0.18	0.13	0.08	0.06	0.03	0.06	n.d.	0.14	0.13
Al_2O_3	11.32	11.25	10.15	10.21	11.68	10.43	1.39	0.71	11.61	10.65
Fe_2O_3**	5.85	6.36	6.55	7.89	4.51	5.78	1.88	3.72	2.72	4.66
FeO	1.80	1.42	3.86	4.34	4.59	4.70	9.52	8.27	7.50	6.99
MnO	0.03	0.04	0.11	0.17	0.02	0.08	0.18	0.24	0.05	0.11
MgO	15.46	15.38	14.46	13.19	11.72	11.78	16.60	17.21	13.64	12.92
CaO	6.74	6.48	7.23	6.54	1.38	2.10	11.77	11.94	8.53	7.47
Na_2O	4.41	4.36	3.95	3.95	6.25	5.84	0.43	0.39	4.18	4.08
K_2O	0.27	0.22	0.27	0.23	0.02	0.04	0.03	0.02	0.48	0.23
H_2O**	2.16	2.16	2.13	2.12	2.23	2.19	2.13	2.14	2.08	2.11
F	n.d.	n.d.	n.d.	n.d.	n.d.	n.d.	n.d.	n.d.	n.d.	n.d.
Cl	0.06	0.08	0.09	0.07	0.02	0.01	n.d.	n.d.	0.07	0.01
O=F	n.d.	n.d.	n.d.	n.d.	n.d.	n.d.	n.d.	n.d.	n.d.	n.d.
O=Cl	–0.01	–0.02	–0.02	–0.02	0.00	0.00	n.d.	n.d.	–0.02	0.00
Σ	100.19	100.34	100.52	100.19	100.83	99.84	100.49	101.00	99.63	99.62
Si	7.16	7.19	7.18	7.20	7.83	7.77	7.94	7.90	6.94	7.12
$Al^{(IV)}$	0.84	0.81	0.82	0.80	0.17	0.23	0.06	0.10	1.06	0.88
M (123)										
$Al^{(VI)}$	1.00	1.01	0.84	0.88	1.68	1.46	0.17	0.01	0.89	0.91
Ti	0.01	0.02	0.01	0.01	0.01	<0.01	0.01	n.d.	0.01	0.01
Fe^{3+}	0.61	0.66	0.69	0.83	0.45	0.59	0.20	0.39	0.29	0.50
Fe^{2+}	0.21	0.16	0.45	0.51	0.52	0.54	1.12	0.97	0.89	0.83
Mn	<0.01	0.01	0.01	0.02	<0.01	0.01	0.02	0.03	0.01	0.01
Mg	3.17	3.15	3.00	2.75	2.34	2.40	3.48	3.60	2.90	2.73
M (4)										
Ca	0.99	0.95	1.08	0.98	0.20	0.31	1.77	1.79	1.30	1.14
Na	1.01	1.05	0.92	1.02	1.63	1.55	0.12	0.11	0.70	0.86
A-site										
Na	0.17	0.11	0.14	0.05	0.00	0.00	0.00	0.00	0.46	0.26
K	0.05	0.04	0.05	0.04	n.d.	0.01	0.01	0.00	0.09	0.04
OH	1.99	1.98	1.98	1.98	2.00	2.00	2.00	2.00	1.98	2.00
F	n.d.	n.d.	n.d.	n.d.	n.d.	n.d.	n.d.	n.d.	n.d.	n.d.
Cl	0.01	0.02	0.02	0.02	n.d.	n.d.	n.d.	n.d.	0.02	n.d.

*Formulae normalized to 13 small cations excluding Na, K, Ca in the A-site; **—calculated; n.d.—not detected.
[1 - 8] represent a profile through an amphibole in an eclogite from core to rim; [1 - 4] barroisite core [1] inner core - [4] outer core; [5, 6] glaucophane , [5] inner rim, [6] outer rim; [7, 8] outermost actinolite rim, sample IBSF 10; [9] amphibole inclusion in garnet and [10] matrix amphibole coexisting with garnet from a garnet amphibolite layer, sample IBSF34.

11–13 mol%. Some epidote inclusions in amphiboles from the eclogites and the massive amphibolites show cores with significant La, Ce and Nd contents (Table 5).

Paragonite and muscovite: Representative analyses are shown in Table 6. The K-content [100·K/(K + Na)] of the matrix paragonite porphyroblasts ranges from 7 to 12. Muscovite (Si = 6.15–6.40 apfu) coexists with paragonite in a few samples (IBSF 4, IBSF 40) within the high-pressure assemblage clinozoisite + zoisite + omphacite + quartz, but in most cases muscovite is only part of the late greenschist-facies stage. Na-contents of the high-pressure muscovite range from 12 to 14 mol%, and the Na-content of coexisting paragonite is 95 mol%, suggesting that the two micas equilibrated, as shown by GIORGETTI et al. (2000). Greenschist-facies muscovite overgrew paragonite across grain boundaries (Fig. 4K). Its Na-content is low (4 mol%), below the corresponding K-content in paragonite (8–11 mol%), suggesting disequilibrium growth (GIORGETTI et al., 2000). No F and very little Cl are found in the micas, although the late muscovite has significant Ba-contents (0.7–0.8 wt% BaO). Transmission electron microscope (TEM) investigations on the late stage muscovite indicate that it is a disordered 2M-polytype (GIORGETTI et al., 2000).

Table 3 (cont.) Representative electron microprobe analyses of amphibole.

	11 Barr.	12 Gln.	13 Act.	14 Barr.	15 Barr.	16 Barr.	17 Barr.	18 Barr.	19 Barr.	20 Barr.
SiO_2	50.98	57.44	56.23	51.66	51.68	47.66	46.54	47.61	46.39	48.32
TiO_2	0.19	0.03	n.d.	0.18	0.16	0.37	0.28	0.25	0.21	0.23
Al_2O_3	10.75	11.67	1.84	11.81	11.53	12.93	13.91	13.21	12.81	10.05
Fe_2O_3**	2.41	2.26	0.42	3.14	3.31	1.93	4.68	3.40	2.42	4.44
FeO	7.05	6.22	8.44	4.42	3.71	7.31	7.31	6.64	6.92	6.64
MnO	0.09	0.01	0.18	0.11	0.14	0.12	0.11	0.18	0.11	0.07
MgO	13.86	11.51	17.86	14.83	15.04	13.80	12.20	13.25	14.16	14.29
CaO	7.53	1.38	12.05	6.76	6.77	9.53	8.28	9.02	10.17	9.76
Na_2O	4.46	6.81	0.81	5.08	4.80	3.64	4.26	3.58	3.41	3.01
K_2O	0.30	0.03	0.04	0.30	0.30	0.45	0.55	0.46	0.61	0.39
H_2O**	2.09	2.20	2.13	2.15	2.14	2.10	2.10	2.10	2.07	2.08
F	n.d.	n.d.	n.d.	n.d.	n.d.	n.d.	n.d.	n.d.	n.d.	n.d.
Cl	0.14	0.01	0.01	0.06	0.06	0.04	0.01	n.d.	0.08	0.06
O=F	n.d.	n.d.	n.d.	n.d.	n.d.	n.d.	n.d.	n.d.	n.d.	n.d.
O=Cl	–0.03	0.00	0.00	–0.01	–0.01	0.00	0.00	n.d.	–0.02	–0.02
Σ	99.82	99.55	99.99	100.48	99.64	99.87	100.30	99.72	99.41	99.40
Si	7.19	7.84	7.90	7.15	7.18	6.78	6.64	6.77	6.66	6.93
$Al^{(IV)}$	0.81	0.16	0.10	0.85	0.82	1.22	1.36	1.23	1.34	1.07
M (123)										
$Al^{(VI)}$	0.97	1.71	0.20	1.07	1.07	0.95	0.98	0.99	0.83	0.63
Ti	0.02	<0.01	n.d.	0.02	0.02	0.04	0.03	0.03	0.02	0.02
Fe^{3+}	0.26	0.23	0.04	0.33	0.35	0.21	0.50	0.36	0.26	0.48
Fe^{2+}	0.83	0.71	0.99	0.51	0.43	0.87	0.87	0.79	0.83	0.80
Mn	0.01	<0.01	0.02	0.01	0.02	0.01	0.01	0.02	0.01	0.01
Mg	2.91	2.34	3.74	3.06	3.12	2.92	2.59	2.81	3.03	3.05
M (4)										
Ca	1.14	0.20	1.81	1.00	1.01	1.45	1.27	1.38	1.56	1.50
Na	0.86	1.80	0.19	1.00	0.99	0.55	0.73	0.62	0.44	0.50
A-site										
Na	0.36	<0.01	0.03	0.36	0.30	0.46	0.44	0.36	0.52	0.34
K	0.05	<0.01	0.01	0.05	0.05	0.08	0.10	0.08	0.11	0.07
OH	1.97	2.00	2.00	1.99	2.00	1.99	2.00	2.00	1.98	1.99
F	n.d.	n.d.	n.d.	n.d.	n.d.	n.d.	n.d.	n.d.	n.d.	n.d.
Cl	0.03	n.d.	n.d.	0.01	n.d.	0.01	n.d.	n.d.	0.02	0.01

[11 - 13] represent a profile through an amphibole porphyroblast in an eclogite facies vein from core to rim; [11] barroisite core; [12] glaucophane rim; [13] outermost actinolite rim, sample IBSF 22A; [14] amphibole with rutile and dolomite inclusions in core and [15] matrix amphibole without any inclusions coexisting with garnet, sample IBSF 4; [16 - 20] amphiboles from the massive amphibolites, [16] sample IBSF 14, [17] sample IBSF 27 AB, [18] sample IBSF 13 and [19, 20] sample IBSF 17.

Minor minerals: The texturally earliest carbonate is a ferroan dolomite with a Mg# [100·Mg/(Mg + Fe^{2+})] of 85–90. Calcite replacing dolomite contains (Fe+Mg) < 0.02 apfu (Table 7). Carbonates contain also minor amounts of Sr and Ba (Table 7). Talc is ferroan with a low Mg# of 86–87 (Table 8). Chlorite that replaced glaucophane or garnet in the eclogites is ferroan clinochlore (Table 8). In the amphibole-rich bodies, chlorite shows an increase in Fe from cores to rims. Secondary plagioclase is almost pure albite (Ab_{98}–Ab_{99}, Table 9). Titanite shows minor F, Al, Nb, Ta and Ce contents (Table 5).

6. Thermobarometry

The metamorphic evolution of most high-grade rocks is a dynamic process, leading to a series of sequential mineral assemblages. Exchange ther-

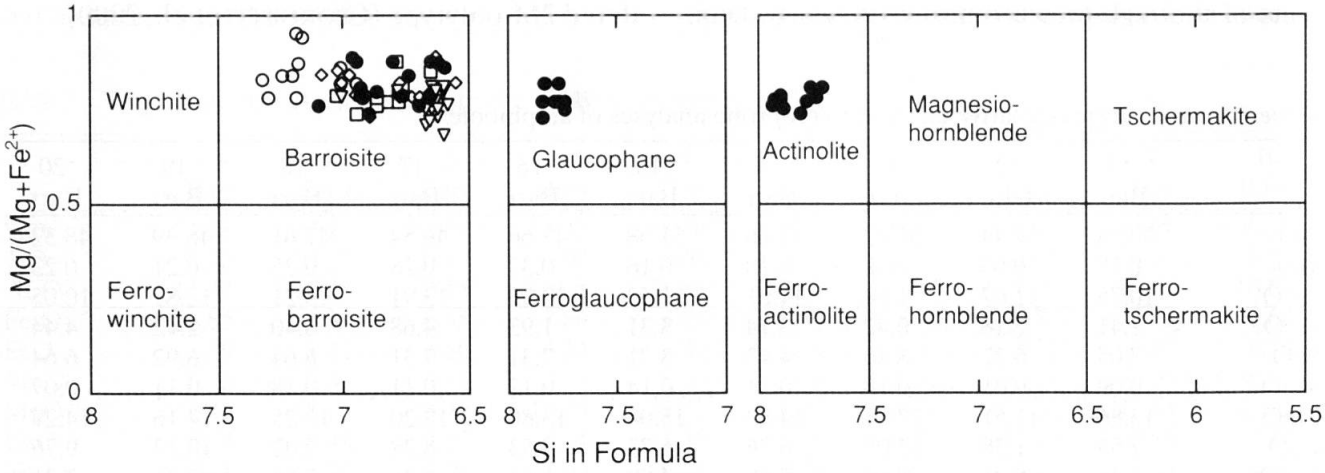

Fig. 7 Amphibole classification according to LEAKE et al. (1997). Left: Na-Ca amphiboles; open circles: barroisite from eclogites, all other symboles: barroisite from amphibolites. Middle: Na-amphiboles; filled circles: glaucophanes from eclogites. Right: Ca-amphiboles; filled circles: actinolites from eclogites.

Table 4 Representative electron microprobe analyses of clinozoisite and zoisite*.

	1 Czo.	2 Czo.	3 Zo.	4 Czo.	5 Zo.	6 Czo.	7 Zo.	8 Czo.	9 Czo.
SiO_2	39.27	39.47	39.70	38.84	39.93	38.63	39.15	38.60	38.81
TiO_2	0.09	0.08	0.03	0.06	n.d.	0.09	0.04	0.09	0.04
Al_2O_3	27.91	28.80	31.59	26.73	32.02	26.25	30.73	27.27	25.86
Fe_2O_3	7.62	5.69	2.61	8.73	1.93	9.08	2.94	8.08	9.74
MnO	0.03	n.d.	0.08	0.02	0.03	0.14	0.08	0.06	0.11
CaO	23.53	23.63	24.25	23.54	24.46	23.37	24.49	23.81	23.44
H_2O**	1.94	1.94	1.97	1.92	1.98	1.91	1.95	1.92	1.91
Σ	100.40	99.62	100.24	99.84	100.36	100.36	99.37	99.37	99.91
Si	3.03	3.05	3.02	3.03	3.03	3.03	3.01	3.02	3.04
Al	2.54	2.62	2.83	2.46	2.86	2.43	2.79	2.50	2.39
Ti	<0.01	<0.01	<0.01	<0.01	n.d.	0.01	<0.01	0.01	<0.01
Fe^{3+}	0.44	0.33	0.15	0.51	0.11	0.54	0.17	0.47	0.57
Mn	<0.01	n.d.	<0.01	<0.01	<0.01	0.01	<0.01	<0.01	0.01
Ca	1.95	1.96	1.98	1.97	1.99	1.97	2.02	1.99	1.97
OH**	1.00	1.00	1.00	1.00	1.00	1.00	1.00	1.00	1.00

*Formulae normalized to 12.5 O + 1 OH assuming all Fe is Fe^{3+}; **—calculated; n.d.—not detected.
Analyses of clinozoisite inclusions in garnet cores from samples IBSF 10 [1] and IBSF 19B [2]; coexisting zoisite [3] and clinozoisite [4] in the matrix of sample IBSF 4; coexisting zoisite [5] and clinozoisite [6] in the core of a garnet in sample IBSF 71; coexisting zoisite [7] and clinozoisite [8] in a late stage eclogite-facies vein crosscutting the main foliation, IBSF 61VI; [9] clinozoisite rim analyses from sample IBSF 4.

mometry and phase equilibrium calculations have been applied to assemblages that were believed to be in textural equilibrium. In some cases, especially for the blueschist- and greenschist-facies assemblages where the assumption of textural equilibrium is questionable and the high variance does not permit accurate *P-T* estimates, these calculations provide only limits. Thermobarometric calculations using selected equilibria in the system Na_2O–CaO–FeO–MgO–Al_2O_3–SiO_2–H_2O (NCFMASH) have been applied to mineral assemblages from five different stages of the *P-T* path. The phase equilibria have been calculated by using the data base of HOLLAND and POWELL (1998) and their updated software THERMOCALC v. 2.7 (HOLLAND 1999, unpubl.). The activity models for most phases were calculated with the program *AX* (HOLLAND, 1999, unpubl.). For garnet, we used the comprehensive quaternary model of GANGULY et al. (1996). For pyroxene, we applied the quaternary model of HOLLAND (1990) and for zoisite the activity of $Ca_2Al_3Si_3O_{12}(OH)$ was taken as X_{Al} on M(3) according to EVANS (1990).

Table 5 Representative electron microprobe analyses of REE-bearing epidote and titanite*.

	1 Aln.	2 Aln.	3 Aln.	4 Ttn.	5 Ttn.	6 Ttn.
SiO_2	37.81	38.08	37.94	30.44	30.47	30.02
TiO_2	0.10	0.07	0.10	37.33	39.21	37.90
Al_2O_3	27.40	27.38	26.38	1.58	0.59	1.29
Cr_2O_3	0.02	n.d.	n.d.	0.14	n.d.	n.d.
Fe_2O_3	6.78	7.31	8.90	0.32	0.47	1.03
La_2O_3	0.34	0.34	0.19	n.d.	n.d.	n.d.
Ce_2O_3	0.99	0.92	0.43	0.09	0.10	0.05
Nd_2O_3	1.06	0.89	0.25	n.d.	n.d.	n.d.
Y_2O_3	n.d.	n.d.	0.21	n.d.	n.d.	n.d.
Nb_2O_5	n.d.	n.d.	n.d.	0.02	0.10	0.05
Ta_2O_5	n.d.	n.d.	n.d.	0.23	0.08	0.28
MgO	0.26	0.29	0.16	n.d.	n.d.	n.d.
MnO	0.06	n.d.	0.01	n.d.	n.d.	0.05
CaO	21.95	22.33	22.30	28.23	27.91	28.00
SrO	0.30	0.18	0.41	0.02	n.d.	0.02
F	n.d.	n.d.	n.d.	0.37	0.27	0.32
H_2O**	1.87	1.90	1.92	0.07	0.01	0.10
O=F	n.d.	n.d.	n.d.	0.16	0.11	0.13
Σ	98.93	99.67	99.21	98.75	99.12	98.96
Si	3.00	3.00	3.00	1.00	1.00	1.00
Al	2.46	2.55	2.47	0.06	0.02	0.05
Ti	0.01	<0.01	0.01	0.92	0.97	0.94
Cr	<0.01	n.d.	n.d.	<0.01	n.d.	n.d.
Fe^{3+}	0.30	0.38	0.42	0.01	0.01	0.03
Fe^{2+}	0.05	0.05	0.12	n.d.	n.d.	n.d.
La	0.01	0.01	<0.01	n.d.	n.d.	n.d.
Ce	0.03	0.03	0.01	<0.01	<0.01	<0.01
Nd	0.03	0.03	0.01	n.d.	n.d.	n.d.
Y	n.d.	n.d.	0.11	n.d.	n.d.	n.d.
Nb	n.d.	n.d.	n.d.	<0.01	<0.01	<0.01
Ta	n.d.	n.d.	n.d.	<0.01	<0.01	<0.01
Mg	0.03	0.03	0.02	n.d.	n.d.	n.d.
Mn	<0.01	n.d.	<0.01	n.d.	n.d.	<0.01
Sr	0.01	0.01	0.02	<0.01	n.d.	<0.01
Ca	1.87	1.89	1.90	0.99	0.98	0.99
F	n.d.	n.d.	n.d.	0.04	0.03	0.03
OH**	0.99	1.00	1.01	0.03	0.01	0.04

*Formulae normalized to 3 Si for clinozoisite and 1 Si cation for titanite; Fe^{2+} in clinozoisite has been calculated according to Fe^{2+} = Σ REE + Ti – Mg – Mn.
**—calculated; n.d.—not detected.
[1, 2, 3] analyses of late eclogite facies clinozoisite cores from inclusions in barroisites, [1] sample IBSF4, [2, 3] sample IBSF 19B; [4, 5, 6] analyses of Al-bearing titanites rimming rutiles, [4] sample IBSF 61 VI, [5, 6] sample IBSF 10.

6.1. INCLUSION ASSEMBLAGE IN GARNET CORE (HIGH-PRESSURE STAGE I, HP I)

In a few garnet cores, the assemblage clinozoisite/zoisite + quartz + kyanite ± paragonite is found. Since Ca- and Na-bearing precursor minerals (anorthite, lawsonite, albite) are missing from the assemblage, it is only possible to calculate P-T limits for the assemblage clinozoisite/zoisite + kyanite + quartz based on the reactions listed in Appendix 2. Reactions (1a,b) provide an upper pressure, and reactions (2) and (3a,b) provide only lower pressure limits, because the activity of $CaAl_2Si_2O_8$ is not constrained. Equilibrium (3a,b) yields very low limiting pressures of ca. 7–9 kbar at 600 °C. Only one sample (IBSF 71) could be used to calculate the *P-T* conditions of the garnet cores. Calculations involving reaction (4a,b) in sample IBSF 71, yields pressures of 21–23 kbar at temperatures of 600–650 °C; these are outside the stability limit of paragonite according to reaction (6). The paragonite-breakdown reaction (6) puts an upper pressure constraint for this assemblage in the absence of omphacite (Fig. 8A). Unfortunately, these equilibria involve H_2O, and since no additional constraint is provided on $a(H_2O)$, the calculations were performed assuming $a(H_2O)$ = 1. The positions of equilibria (4a,b), which are above the paragonite breakdown reaction (6) indicate that $a(H_2O)$ has to be lower than 1 to shift these curves into the paragonite stability field. The lawsonite breakdown curves (1a,b) provide a lower temperature limit as shown in Fig. 8A. Due to the occurrence of zoisite, a lower pressure constraint comes from reaction (5b) in the NCMASH system which involves zoisite, and limits pressures to at least 17–18 kbar between 600–650 °C.

6.2. INNER GARNET RIM INCLUSION ASSEMBLAGE (HIGH-PRESSURE STAGE II, HP II)

Temperature estimates have been obtained with Fe^{2+}–Mg exchange thermometry between garnet and clinopyroxene with the most recent calibration of KROGH RAVNA (2000a). The temperatures obtained from 28 pairs of garnets coexisting with clinopyroxene inclusions in the garnets yields temperatures ($\pm 1\sigma$) of 590 ± 10 °C (sample IBSF 19B), 640 ± 10 °C (sample IBSF 71), 570 °C (sample IBSF 61), 620 ± 40 °C (sample IBSF 10) and 610 ± 40 °C (sample IBSF 22A).

H_2O-free phase equilibrium calculations: The assemblage garnet + omphacite + kyanite + clinozoisite + quartz ± zoisite permits the calculation of several H_2O-free equilibria in the NCMASH or NCFASH as listed in Appendix 2. Intersecting reactions (7a), (7b) and the steep Fe^{2+}–Mg exchange reaction between garnet and omphacite (8) results in a *P–T* estimate, that is independent on $a(H_2O)$. We used coexisting garnet and omphacite and the *P-T* estimates obtained from four inclusion assemblages in garnet rims (sample IBSF 10, IBSF 71, IBSF 19B, IBSF 61VI) yield 550 °C to 645 °C and 19 to 21 kbar as shown in Fig. 8B.

H_2O-bearing phase equilibrium calculations: The equilibria involving an OH-bearing phase such as clinozoisite/zoisite and a fluid phase yields

Table 6 Representative electron microprobe analyses of muscovite and paragonite*.

	1 Ms.	2 Pg.	3 Ms.	4 Pg.	5 Pg.	6 Pg.	7 Pg.	8 Pg.	9 Pg.
SiO_2	48.49	46.34	49.05	45.93	45.55	46.89	46.49	46.25	47.76
TiO_2	0.24	0.04	0.06	0.10	0.04	0.04	0.07	0.13	0.03
Al_2O_3	29.21	39.39	29.93	40.07	39.85	39.67	39.55	39.64	39.17
Cr_2O_3	n.d.	n.d.	0.03	n.d.	n.d.	n.d.	n.d.	n.d.	0.03
Fe_2O_3	2.00	0.69	2.26	0.70	0.92	0.47	0.37	0.43	0.56
FeO	0.30	n.d.	0.01	n.d.	n.d.	0.04	n.d.	n.d.	n.d.
MnO	n.d.	0.03	0.01	n.d.	0.05	n.d.	0.02	0.03	n.d.
MgO	2.87	0.17	2.52	0.20	0.18	0.20	0.23	0.17	0.16
CaO	0.01	0.20	0.03	0.32	0.69	0.46	0.37	0.35	0.33
BaO	0.53	n.d.	0.26	n.d.	0.09	0.08	n.d.	0.06	n.d.
Na_2O	1.04	7.53	0.29	6.57	7.19	7.48	7.19	7.35	6.88
K_2O	10.06	0.65	10.79	1.30	0.68	0.61	0.76	0.84	0.85
H_2O**	4.48	4.69	4.50	4.70	4.68	4.68	4.70	4.68	4.70
F	n.d.	n.d.	n.d.	n.d.	n.d.	n.d.	n.d.	n.d.	0.01
Cl	0.02	0.01	0.01	0.03	<0.01	n.d.	<0.01	<0.01	n.d.
O=F	n.d.	n.d.	n.d.	n.d.	n.d.	n.d.	n.d.	n.d.	<0.01
O=Cl	–0.01	0.00	0.00	–0.01	0.00	n.d.	0.00	0.00	n.d.
Σ	99.25	99.73	99.75	99.91	99.90	100.64	100.28	99.95	100.47
Si	6.53	5.94	6.55	5.86	5.84	5.96	5.95	5.93	6.06
$Al^{(IV)}$	1.47	2.06	1.45	2.14	2.16	2.04	2.05	2.07	1.94
$Al^{(VI)}$	3.16	3.89	3.26	3.89	3.87	3.91	3.91	3.91	3.91
Ti	0.02	<0.01	0.01	0.01	<0.01	<0.01	0.01	0.01	<0.01
Cr	n.d.	n.d.	<0.01	n.d.	n.d.	n.d.	n.d.	n.d.	<0.01
Fe^{3+}	0.20	0.07	0.23	0.07	0.09	0.05	0.04	0.04	0.05
Fe^{2+}	0.03	n.d.	<0.01	n.d.	n.d.	<0.01	n.d.	n.d.	n.d.
Mn	n.d.	<0.01	<0.01	n.d.	0.01	n.d.	<0.01	<0.01	n.d.
Mg	0.58	0.03	0.50	0.04	0.03	0.04	0.04	0.03	0.03
Ba	0.03	n.d.	0.01	n.d.	<0.01	<0.01	n.d.	<0.01	n.d.
Ca	<0.01	0.03	<0.01	0.04	0.09	0.06	0.05	0.05	0.04
Na	0.27	1.87	0.08	1.63	1.79	1.84	1.78	1.83	1.69
K	1.73	0.11	1.84	0.21	0.11	0.10	0.12	0.14	0.14
OH	4.00	4.00	4.00	3.99	4.00	4.00	4.00	4.00	4.00
F	n.d.	n.d.	n.d.	n.d.	n.d.	n.d.	n.d.	n.d.	<0.01
Cl	<0.01	<0.01	<0.01	0.01	<0.01	n.d.	<0.01	<0.01	n.d.

*Formulae normalized to 12 small cations for phengitic white micas; **—calculated; n.d.—not detected.
Coexisting phengitic muscovite [1] and paragonite [2] in sample IBSF 4; greenschist facies phengite [3] replaces matrix paragonite [4], sample IBSF 10; [5] paragonite inclusion in garnet core, paragonite inclusion in omphacite [6], paragonite matrix [7], all from sample IBSF 71; [8], [9] paragonites from late stage eclogite-facies veins from samples IBSF 61VI and IBSF 22A.

an intersection in the NMASH (equilibria 9–11) and corresponding NFMASH system involving H_2O (equilibria 12–14). The estimation of $a(H_2O)$ was performed by using the T estimates obtained above to calculate P-$a(H_2O)$ diagrams with the intersections described above as shown in Fig. 8C. The resulting $a(H_2O)$ ranges from 0.39–0.81 in the four samples (Fig. 8C, Table 10). The pistacite content of clinozoisite inclusions in garnet varies from 11 to 19 mol%. The H_2O-involving equilibria all include clinozoisite, and $a(H_2O)$ depends strongly on the activity of $Ca_2Al_3Si_3O_{12}(OH)$, which can vary ± 0.2 in a sample, probably implicating local small-scale variations of $a(H_2O)$ for some inclusion assemblages.

6.3. LATE ECLOGITE-FACIES MATRIX ASSEMBLAGE (HIGH-PRESSURE STAGE III, HP III)

H_2O-free phase equilibrium calculations: Overall, it is more difficult to estimate the P-T conditions of the strongly hydrated stage of the eclogite-facies, since (1) the thermodynamic data for barroisite are not well constrained and (2) retrogression occurs pervasively over a thin section. The latter affects mostly garnets and leads to a wide range in Fe^{2+}/Mg ratios in the garnets which grew together with barroisites and omphacites. Omphacite also shows a wide range in Fe^{2+}/Mg ratios although it lacks healed fractures with compositional changes. Therefore, the temperatures obtained from 48 coexisting garnet-matrix pyroxene pairs, yielded a wide range of temperatures of 400–600 °C. In Fig. 8D, the light grey area only shows the range of garnet-clinopyroxene temperatures of garnet-clinopyroxene pairs which were not thought to be affected by retrogression. Garnet-hornblende thermometry with the calibration of GRAHAM and POWELL (1984) was applied to 21 garnet-amphibole pairs from (1.) amphibole inclusions in garnet rims and (2.) coexisting garnet-amphibole pairs. The temperatures (± 1σ) obtained from amphibole inclusions in garnet are 610 ± 10 °C (sample IBSF 34) and the coexisting garnet-barroisite pairs yield 590 ± 20 °C (sample IBSF 19B) and 550 ± 30 °C (sample IBSF 4). The chemical composition of the amphiboles used in this study deviates from those used in the calibration by GRAHAM and POWELL (1984), since they contain slightly higher Na contents on the M(4) site, thus introducing an additional uncertainty which is difficult to evaluate. KROGH RAVNA (2000b) also recalibrated the garnet-hornblende thermometer based on synthetic and natural amphiboles. This new calibration yields temperatures of 370 to 490 °C, which seems too low, compared with the garnet-clinopyroxene thermometry.

Table 7 Representative electron microprobe analyses of dolomite and calcite*.

	1 Dol.	2 Dol.	3 Dol.	4 Dol.	5 Cal.	6 Cal.
CaO	28.61	28.82	28.48	29.00	55.00	54.89
MgO	19.86	19.36	18.47	18.50	0.30	0.20
FeO	4.07	3.83	5.78	4.78	0.15	1.18
MnO	0.12	0.14	0.06	n.d.	0.43	0.24
SrO	0.02	0.05	0.14	0.15	0.10	0.09
BaO	n.d.	0.18	0.15	0.08	0.09	0.03
CO_2**	46.72	47.49	46.20	45.97	43.92	44.21
Σ	99.40	98.63	99.28	98.49	100.00	100.84
Ca	0.96	0.98	0.97	0.99	0.99	0.97
Mg	0.93	0.91	0.87	0.88	0.01	<0.01
Fe	0.11	0.10	0.15	0.13	<0.01	0.02
Mn	<0.01	<0.01	<0.01	n.d.	<0.01	<0.01
Sr	<0.01	<0.01	<0.01	<0.01	<0.01	<0.01
Ba	n.d.	<0.01	<0.01	<0.01	<0.01	<0.01
Mg#	0.89	0.90	0.85	0.87	-	-

*Formulae of dolomites normalized to 2 cations and calcite formulae normalized to 1 cation; Mg#: Mg/(Mg+Fe^{2+}); **CO_2 content calculated by stoichiometry; n.d. – not detected.
Dolomite inclusions in core of amphibole nodule in late stage eclogite facies vein [1, 2], sample IBSF 22A; [3, 4] dolomite inclusions in omphacite, sample IBSF 58 VI, [5, 6] calcite replacing dolomite [1, 2] in sample IBSF 22 A.

H_2O-bearing phase equilibrium calculations: Kyanite is not present in the matrix, and the P-T conditions are therefore based on equilibria (15)–(18) from Appendix 2 involving garnet, clinopyroxene, clinozoisite, zoisite, quartz and H_2O. For these calculations we used the garnet rims, which have amphibole inclusions (samples IBSF 61 VI, IBSF 19B/2), or small garnets growing along the cleavage of the barroisite porphyroblasts which also coexist with omphacite (samples IBSF 58 VI, IBSF 22A). Only in samples IBSF 10 and IBSF 40, we used the outermost rims of garnet porphyroblasts, coexisting with matrix omphacites. Since a slight decrease in the grossular content between the garnets growing along veins in barroisite and omphacite porphyroblasts and the garnets growing in the first stage of the eclogite-facies occurs, the calculated pressures are expected to be slightly lower. The pressures and temperatures obtained with the intersection of equilibria (15)–(17) from 6 samples with the assumption of $a(H_2O) = 1$, are 16–21 kbar and 570–650 °C (Table 10; Fig. 8D).

The calculation of $a(H_2O)$ is difficult because $a(H_2O)$ is very sensitive to uncertainties in the temperature estimates. Due to these uncertain-

ties, no attempt has been made to calculate $a(H_2O)$ with equilibria among the phases garnet, clinopyroxene, clinozoisite, zoisite, quartz and H_2O. In addition to the OH-bearing minerals barroisite, paragonite and zoisite, CO_2-bearing minerals such as dolomite also coexist with the assemblage garnet + omphacite + barroisite + paragonite + clinozoisite + quartz ± zoisite thus indicating the presence of a mixed fluid in the system H_2O–CO_2. The presence of dolomite allows an estimate of $X(CO_2)$ and $X(H_2O)$ of the fluid in equilibrium with the eclogite-facies matrix assemblage if the fluid is represented by the H_2O–CO_2 binary. This assumption is reasonable in light of the significant Fe^{3+} contents of epidote (DONOHUE and ESSENE, 2000). Ultimately, this allows the calculation of $a(H_2O)$ and $a(CO_2)$ by using the equation of state for the system H_2O–CO_2 by HOLLAND and POWELL (1991) with the program RK (CONNOLLY, 1999; written comm.). This allows to calculate limits of $a(H_2O)$ of the fluid by calculating P-$X(CO_2)$ diagrams involving equilibria (19)–(21) among garnet, omphacite, clinozoisite/zoisite, dolomite, quartz, H_2O and CO_2 as shown in Appendix 2, at temperatures ranging from 550 °C to 650 °C. Equilibria among this assemblage yield an intersection which yields low $X(CO_2)$ contents, ranging from 0.02 at 20 kbar to 0.20 at 14 kbar (sample IBSF 19B/2) and 0.04 at 18 kbar to 0.11 at 14 kbar (sample IBSF 58VI). The lower pressure limit of 14 kbar was taken from the lower stability limit of omphacite according to reaction (18). The resulting $a(H_2O)$ yields high values of 0.84–0.98 (Table 10). Due to the fact that only limits of $a(H_2O)$ were calculated, the calculation of the invariant points in Fig. 8C was performed with the assumption of $a(H_2O) = 1$.

Table 8 Representative electron microprobe analyses of chlorite and talc*.

	1 Chl.	2 Chl.	3 Chl.	4 Chl.	5 Chl.	6 Tlc.	7 Tlc.
SiO_2	28.32	29.29	30.15	29.04	29.65	61.06	61.07
TiO_2	0.07	0.02	0.01	n.d.	0.02	0.08	n.d.
Al_2O_3	19.02	19.82	19.62	20.20	20.48	0.41	0.47
FeO	20.02	16.40	13.48	16.85	14.07	8.13	7.57
MnO	0.31	0.11	0.16	0.30	0.12	n.d.	n.d.
MgO	19.53	21.53	23.91	20.99	22.97	26.14	25.78
CaO	0.10	0.38	0.01	0.02	0.02	0.20	0.37
Na_2O	0.02	n.d.	n.d.	0.02	0.02	0.09	0.19
K_2O	0.01	n.d.	n.d.	n.d.	n.d.	n.d.	n.d.
H_2O**	11.81	12.04	12.22	12.02	12.19	4.57	4.59
Cl	0.01	0.03	0.02	0.02	0.03	0.02	n.d.
O=Cl	-0.01	-0.01	-0.01	-0.01	-0.01	-0.01	n.d.
Σ	99.20	99.61	99.59	99.46	99.55	100.69	100.05
Si	2.90	2.93	2.97	2.91	2.93	3.98	3.99
$Al^{(IV)}$	1.10	1.07	1.03	1.09	1.07	0.02	0.01
$Al^{(VI)}$	1.20	1.27	1.25	1.31	1.32	<0.01	0.02
Ti	0.01	<0.01	<0.01	n.d.	<0.01	0.01	n.d.
Fe^{2+}	1.72	1.37	1.11	1.41	1.16	0.44	0.42
Mn	0.03	0.01	0.01	0.03	0.01	n.d.	n.d.
Mg	2.98	3.21	3.51	3.14	3.38	2.54	2.51
Ca	0.01	0.04	<0.01	<0.01	<0.01	0.02	0.03
Na	<0.01	n.d.	n.d.	<0.01	<0.01	0.01	0.03
K	<0.01	n.d.	n.d.	n.d.	n.d.	n.d.	n.d.
OH	8.00	8.00	8.00	8.00	8.00	3.99	4.00
Cl	<0.01	<0.01	<0.01	<0.01	<0.01	0.01	n.d.

*Formulae normalized to 12 O + 8 (OH + Cl) for chlorite and to 11 O + 4 (OH + Cl) for talc; **—calculated; n.d.—not detected.
[1, 2] chlorite forming as replacement of barroisite and glaucophane in eclogite sample IBSF 10 and IBSF 22A; [3] chlorite core and [4] chlorite rim analyses from amphibolite sample IBSF 14; [5] chlorite analyses from amphibolite sample IBSF 17; [6, 7] talc forming as replacement of Fe-bearing dolomite in a late stage eclogite facies vein from sample IBSF 22A.

Table 9 Representative electron microprobe analyses of albite*.

	1 Ab.	2 Ab.	3 Ab.
SiO_2	69.00	68.39	68.35
Al_2O_3	19.73	18.88	19.62
Fe_2O_3	0.28	0.16	0.19
MgO	n.d.	0.03	n.d.
CaO	0.34	0.25	0.29
K_2O	n.d.	n.d.	0.03
Na_2O	11.41	11.72	11.64
Σ	100.75	99.40	100.12
Si	2.99	3.01	2.99
Al	1.01	0.98	1.01
Fe^{3+}	0.01	0.01	0.01
Mg	n.d.	<0.01	n.d.
Ca	0.02	0.01	0.01
K	n.d.	n.d.	<0.01
Na	0.96	1.00	0.99
Σ Cations	4.99	5.01	5.01
Ab	0.98	0.99	0.99
Or	0.00	0.00	0.01
An	0.02	0.01	<0.01

*Formulae normalized to 8 oxygens, n.d.—not detected.
Ab: [Na/(Na + K + Ca)], Or: [K/(Na + K + Ca)], An: [Ca/(Na + K + Ca)].
All analyzed albites replace barroisite and glaucophane; [1] sample IBSF 10; [2] sample IBSF 22A; [3] sample IBSF 19B.

6.4. BLUESCHIST-FACIES ASSEMBLAGE

The only indicator for the blueschist-facies is the appearance of glaucophane. Based on textural evidence, it is assumed that glaucophane is in equilibrium with the assemblage clinozoisite + quartz + zoisite, but not with omphacite, paragonite and garnet. The absence of omphacite provides an upper pressure limit according to reaction (18). Reaction (22) has been calibrated experimentally (MARUYAMA et al., 1986) and is used as the boundary reaction between the epidote-blueschist and the greenschist-facies (EVANS, 1990). This reaction provides a lower pressure limit for the blueschist-facies of 8–10 kbar between temperatures of 400 and 500 °C (Fig. 8E). It is more difficult to constrain temperatures for the blueschist-facies because we find no suitable reaction among the phases of the blueschist-facies assemblage. A lower temperature limit for the assemblage glaucophane + clinozoisite can be calculated with a lawsonite-pumpellyite involving reactions (23), since both phases are not stable in these rocks which yields minimum temperatures. In contrast to VENTURINI (1995) and LARDEAUX et al. (1982), we were not able to constrain the temperatures of the blueschist-facies event. These authors were able to deduce temperatures from coexisting garnet-glaucophane pairs and phase equilibrium constraints, which yielded temperatures of 400–500 °C. The upper temperature estimate of VENTURINI (1995) was used as the upper temperature limit. Due to the lack of clear textural relations, no calculations concerning $a(H_2O)$ were performed for the blueschist-facies assemblage.

6.5. GREENSCHIST-FACIES ASSEMBLAGE

The greenschist-facies overprint is pervasive throughout the rocks and replaces minerals from all different stages. Reaction (22) provides an upper pressure limit for the greenschist-facies assemblage actinolite + chlorite + albite + quartz as shown in Fig. 8E. Lower P-T limits of the assemblage clinozoisite + tremolite may be calculated using equilibria involving prehnite and pumpellyite such as (24) and (25) in Appendix 2. These reactions intersect at 260–270 °C and 4 kbar, which provides a minimum estimate for P and T since neither phase is found in the rocks (Fig. 8E). Temperatures were estimated by GIORGETTI et al. (2000) with the muscovite-plagioclase thermometer of GREEN and USDANSKY (1986). This yielded 300 ± 30 °C at 5 ± 2 kbar. Pressures were estimated with reaction (26) among the greenschist-facies assemblage clinochlore + clinozoisite + quartz + tremolite + anorthite. P-T conditions for the greenschist-facies assemblage are therefore at 300 ± 50 °C and between 3 and 6 kbar (Fig. 8E).

The appearance of the assemblage talc + calcite pseudomorphing dolomite in sample IBSF 22A, allows us to constrain $X(CO_2)$ and $X(H_2O)$ and thus to calculate $a(H_2O)$ of the fluid in equilibrium with the greenschist-facies assemblage, using the equilibria in Appendix 2. The value of

Table 10 Thermobarometric results of inclusion and matrix assemblages.

	Sample	Temperature	(±1σ)†	Pressure	(±1σ)	$a(H_2O)$
Gt-rim	IBSF 10	590	21	20.5	2.4	0.81
Inclusions*	IBSF 71	645	22	20.3	2.3	0.81
	IBSF 61VI	550	20	19.1	2.5	0.38
	IBSF 19B/2	602	21	20.9	2.4	0.69
Matrix**	IBSF 19B/2	574	21	19.9	1.7	0.84 – 0.98
	IBSF 58 VI	590	21	17.6	1.8	0.91 – 0.96
	IBSF 22A	567	21	17.6	1.7	0.93 – 0.98
	IBSF 10	622	22	18.6	1.8	—
	IBSF 40	593	22	20.7	1.7	—
	IBSF 61VI	647	25	16.2	1.3	—

*The inclusion assemblage in the garnets (grt + omp + ky + czo + qtz) is used to constrain the conditions of the peak eclogite or first stage of the eclogite-facies conditions. The P-T conditions are based on the intersection involving equilibria (9a), (9b) and (10) from Table 10. The $a(H_2O)$ is calculated by using intersections 1, 2 from the Appendix.

**The matrix assemblage (grt + omp + pg + cz ± zo + qtz) is used to calculate P-T conditions of the late stage or second stage of the eclogite facies conditions by using equilibria (15)–(17) from Table 10. The $a(H_2O)$ is calculated with HOLLAND and POWELL's (1991) CORK equation of state for the system H_2O–CO_2.

†The standard deviations (±1σ) are routinely calculated in the updated (1999) version of THERMOCALC, v. 2.7.

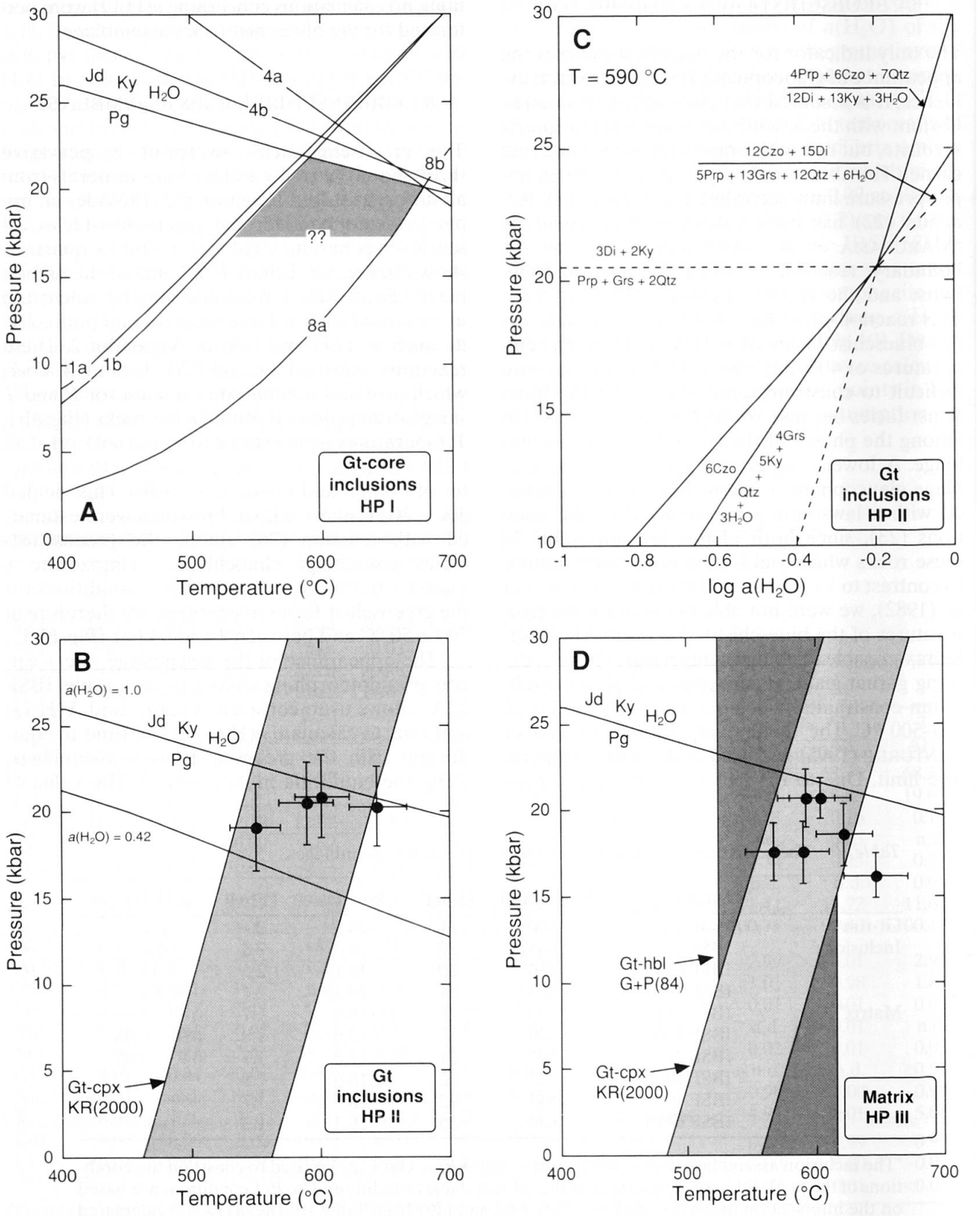

Fig. 8 *P-T* estimates of different stages of the metamorphic path. Note that for clarity, metastable extensions are not indicated on all of the curves in most of these figures.

(A) Early prograde assemblage (high-pressure stage I, HP I), preserved as inclusions in garnet core, sample IBSF 71. Grey shaded area indicates estimated *P-T* conditions. Shown are limiting reactions (1a,b) 4 Lawsonite = 2 Clinozoisite/Zoisite + Kyanite + Quartz + 7 H_2O, and (4a,b) Clinozoisite/Zoisite = Grossular + 2 Kyanite + Quartz + 6 H_2O and reactions (7) Jadeite + Kyanite + H_2O = Paragonite and (8a,b) Grossular + Paragonite + Kyanite + Quartz =

$X(CO_2)$ obtained from reaction (27) is a lower limit because dolomite is not in textural equilibrium with calcite + talc. To estimate $X(CO_2)$ in the fluid in equilibrium with the greenschist-facies assemblage, we calculated P–$X(CO_2)$ diagrams for temperatures ranging from 250 °C to 400 °C. Application of reactions (27) and (28) shows that the assemblage talc + calcite is unstable above 400 °C in the pressure range of 3–6 kbar with respect to tremolite + calcite, thus putting an upper temperature constraint on the greenschist-facies assemblage. Assuming a total pressure range of the greenschist-facies at 300 °C of 3 to 6 kbar, $X(CO_2)$ varies in reaction (28) from 0.001 at 6 kbar to 0.01 at 3 kbar. Overall the resulting $X(CO_2)$ for the greenschist-facies assemblage at pressures between 3–6 kbar is lower than $X(CO_2)$ in the eclogite-facies and the calculated water activity $a(H_2O)$ is high and ranges from 0.98 to 0.99.

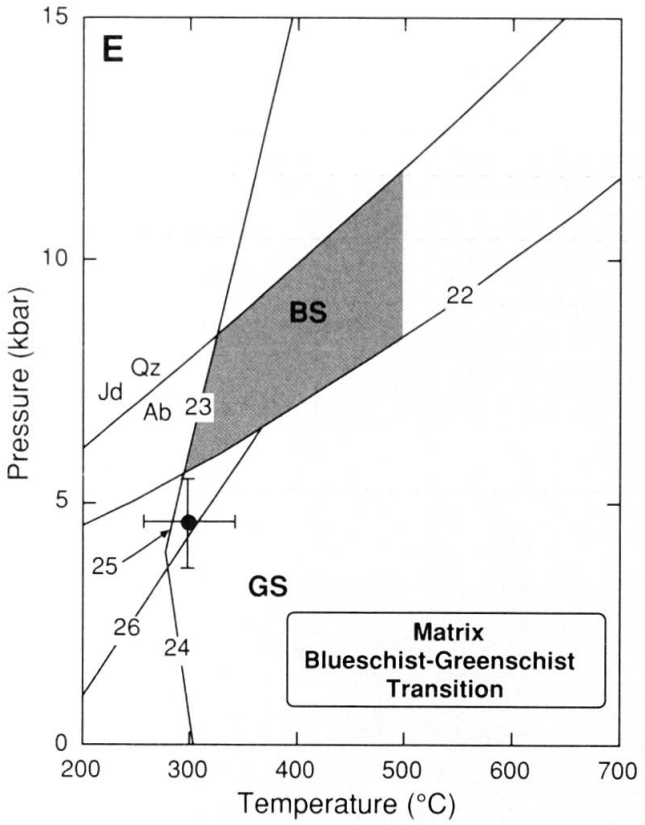

7. Discussion

Compared to previous petrological studies, the eclogites from the Ianca River show a more complex evolution of the eclogite-facies high-pressure stage. This is in part due to changes in external variables, such as $a(H_2O)$. It was possible to obtain $a(H_2O)$ for three stages (high-pressure stage II, high-pressure stage III, greenschist-facies). During the peak eclogite-facies (high-pressure stage II), fluid-undersaturated conditions might be responsible for a lowering of $a(H_2O)$. To obtain $a(H_2O)$ estimates for the late eclogite-facies (high-pressure stage III) and greenschist-facies we assume that free fluid was present based on evidence from fluid inclusions and veins and we simplify the calculation of $a(H_2O)$ by assuming that the coexisting carbonates are an indicator for a mixed H_2O–CO_2 fluid in equilibrium with the assemblages. Although the calculations are only of preliminary nature, they still emphasize the importance of an estimate of $a(H_2O)$ to infer phase relations in hydrated eclogites. This part of the

Fig. 8 (continued)
Clinozoisite/Zoisite + Jadeite. The occurrence of zoisite and thus reaction (8b) involving zoisite, puts a pressure constraint on the inclusion assemblage. Due to the absence of constraints on $a(H_2O)$, the calculations were performed assuming $a(H_2O) = 1$.
(B) Inclusion assemblage in garnet rims (high-pressure stage II, HP II). Grey field shows range of temperatures obtained from garnet-omphacite thermometry (KR 2000: calibration of KROGH RAVNA, 2000a). Equilibrium (6) is calculated with $a(H_2O) = 1.0$ and 0.42 to show the calculated range of $a(H_2O)$. Estimates obtained from four samples shown by error bars.
(C) P–$a(H_2O)$ calculation of inclusion assemblage in garnet rim (high-pressure stage II, HP II) from sample IBSF 10 at 590 °C; the result is $P = 20.5$ kbar and $a(H_2O) = 0.63$. In this figure, metastable extensions are shown.
(D) Matrix assemblage (high-pressure stage III, HP III). Grey field shows temperatures obtained by garnet-omphacite thermometry with the calibration of KROGH RAVNA (2000a, KR 2000); dark grey field shows temperatures obtained by garnet-hornblende thermometry based on GRAHAM and POWELL (1984, G+P 84). Intersections of equilibria (15)–(17) are shown for six samples. Reaction (6) shown as an additional constraint. Calculations assumed $a(H_2O) = 1$.
(E) P-T conditions of blueschist (BS)–greenschist (GS) facies transition in matrix. Grey field indicates range of temperatures for blueschist-facies, obtained from limiting reaction (23) and the upper temperature estimate from VENTURINI (1995). Reactions (22) 25 Glaucophane + 6 Clinozoisite + 14 H_2O + 7 Quartz = 9 Clinochlore + 6 Tremolite + 50 Albite and (18) Albite = Jadeite + Quartz represent pressure limits. The equilibria (24) 2 Clinochlore + 5 Prehnite + 2 Quartz = 4 Clinozoisite + Tremolite + 6 H_2O and (reaction 25) 2 Clinochlore + 25 Pumpellyite + 29 Quartz = 43 Clinozoisite + 7 Tremolite + 67 H_2O provide low temperature limits. Reaction (26) Clinochlore + 6 Clinozoisite + 7 Quartz = Tremolite + 10 Anorthite + 6 H_2O provides another P-T constraint, although not independent of $a(H_2O)$. Black circle with error bars represents the P-T conditions for the greenschist facies assemblage from GIORGETTI et al. (2000).

study has not been documented from the Sesia-Lanzo Zone yet. The best constraints on $a(H_2O)$ are in the garnet rim inclusion assemblages of the high-pressure stage II, where a sufficient number of equilibria make an independent constraint possible (Appendix 2). The occurrence of paragonite as an inclusion in the core of a garnet serves as a monitor for changing $a(H_2O)$ conditions. Paragonite, present as inclusion in the garnet core (high-pressure stage I), disappeared towards the rims of the garnet porphyroblasts (high-pressure stage II) and omphacite + kyanite formed instead. Chemically, there is no evidence in the garnet zoning (e.g. changing pyrope and grossular contents), indicating a coeval increase in pressure or temperature which occurred with the disappearance of paragonite and the formation of omphacite + kyanite. This is probably due to a decrease in $a(H_2O)$ while the garnet grew, thus stabilizing the assemblage omphacite + kyanite. During the subsequent hydration in the eclogite-facies (high-pressure stage III), the pressure dropped slightly, as indicated by lower grossular contents in the outermost garnet rims, and $a(H_2O)$ seems to have increased (0.84–0.98). Therefore the assemblage paragonite + omphacite formed again.

Textural observations and phase equilibrium calculations helped us to constrain the presence of a fluid phase and its activity and composition. The observed textures indicate an episode of vein formation during hydration in the eclogite-facies at still high temperatures and pressures (high-pressure stage III). At first, small (100–500 μm length) garnet + rutile veins formed in omphacite

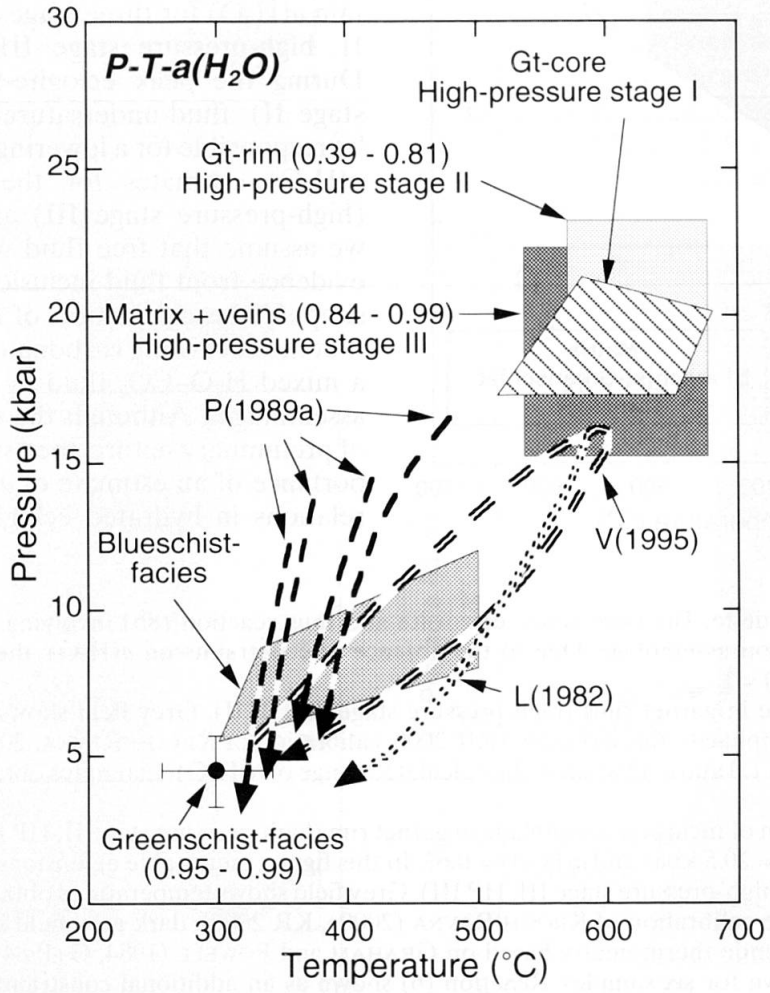

Fig. 9 Comparison of the *P-T-a(H₂O)* path, compiled from thermobarometric results of this study with previously published *P-T* paths from central Sesia-Lanzo Zone by LARDEAUX et al., (1982); L(1982), double stippled line; and VENTURINI (1995); V(1995), double dashed line, and the southern Sesia-Lanzo Zone by POGNANTE (1989a); P(1989a), single dashed line. Numbers in parenthesis show calculated range of $a(H_2O)$ for each stage. Gt-core (shaded area): early prograde inclusion assemblage (high-pressure stage I); Gt-rim (light grea area): peak eclogite inclusion assemblage (high-pressure stage II); Matrix + veins (dark grey area): late stage eclogite-facies assemblage (high-pressure stage III) including paragonite + clinozoisite + zoisite veins crosscutting foliation, which also formed during late stage eclogite-facies. Also shown are results for blueschist facies (middle grey area) and greenschist facies (black circle with error bars) assemblages.

and barroisite porphyroblasts. This stage is also associated with the formation of rutile, zircon and clinozoisite with REE-bearing cores. The occurrence of these veins is restricted and they have been observed in a few samples (IBSF 4, IBSF 58VI) only. The appearance of rutile and zircon inclusions in barroisite cores, and of REE-bearing cores in clinozoisite suggests that the fluid was enriched in Ti, Zr, La, Ce and Nd at the onset of mobilization. The barroisite cores are also rich in Ti (0.2 apfu) indicating that the cores grew in a Ti-rich environment coeval with the growth of rutile. This is consistent with the results of PHILIPPOT and SELVERSTONE (1991), who found fluid inclusions in eclogites that were enriched in Ti, Zr and REE. AYERS and WATSON (1993) also found that an aqueous metamorphic fluid can contain considerable amounts of Ti in solution. Continuing fluid mobilization yielded the formation of macroscopic visible paragonite + clinozoisite + zoisite + barroisite + quartz ± omphacite veins, which crosscut the foliation. These veins also contain barroisite and omphacite porphyroblasts, which contain the garnet veins, as discussed above. The isolated occurrence of the high-pressure veins indicates that fluid mobilization took place only on a localized scale, consistent with observations from other eclogites in the Alps (FRANZ et al., 1989; PHILIPPOT and SELVERSTONE, 1991; SELVERSTONE et al., 1992; NADEAU et al., 1993; GETTY and SELVERSTONE, 1994; BARNICOAT and CARTWRIGHT, 1995; PHILIPPOT et al., 1995). Hydration continued during the subsequent blueschist- and greenschist-facies and seems to have been pervasive, resulting in an extensive overprint during the later stages of the retrograde path, replacing most high-pressure minerals.

The thermobarometric investigation of these multi-stage rocks yields a *P-T* path that indicates a decompression at 550–650 °C from ca. 17–21 kbar down to 300 °C and 3–5 kbar as shown in Fig. 9. This is consistent with previously derived *P-T* paths from the central- and southern Sesia-Lanzo Zone (LARDEAUX et al., 1982; POGNANTE, 1989a; POGNANTE, 1991; VENTURINI, 1995), for which initial almost isothermal decompression and subsequent cooling was inferred (Fig. 9). Most studies agree with this *P-T* path, however, some investigations proposed an increase in temperature with decompression (HUNZIKER, 1974; COMPAGNONI et al., 1977; OBERHÄNSLI et al., 1985). The *P-T* conditions of the peak of the eclogite-facies metamorphism are also in agreement with previous thermobarometric estimates (LARDEAUX et al., 1982; POGNANTE, 1989a; POGNANTE, 1991; VENTURINI, 1995; TROPPER et al., 1999) and the observed mineral assemblages are in agreement with petrogenetic grids obtained from experimental investigations with basaltic protoliths (LIU et al., 1996; MOLINA and POLI, 2000). In contrast to the extensive retrograde overprint, almost no traces of the prograde history remain in eclogites from the Sesia-Lanzo Zone and the prograde *P-T* paths still remains poorly constrained. In this investigation, we only found faint traces of an older garnet relics in a garnet core, but no other hints for the prograde metamorphic evolution. REINSCH (1979), POGNANTE et al. (1980) and VENTURINI (1995) found lawsonite, zoisite amphiboles such as glaucophane and actinolite as inclusions in eclogite garnets; these are considered to be relics of the prograde Alpine evolution. The retrograde decompressional portions of the *P-T* paths from the Sesia-Lanzo Zone are accompanied by a marked temperature decrease. In the southern Sesia-Lanzo Zone, the post-eclogitic evolution led to the formation of lawsonite and later to the formation of albite, epidote, actinolite, stilpnomelane and pumpellyite (POGNANTE, 1989a). In the central Sesia-Lanzo Zone, the temperatures of the peak eclogite-facies conditions were higher, and the retrograde *P-T* path went through a high-*T* blueschist-facies which did not lead to the formation of lawsonite during subsequent decompression and cooling (LARDEAUX et al., 1982; VENTURINI, 1995). Comparison of the retrograde portions of the *P-T* paths of all units from the Western Alps reveals that the easterly and structurally higher units such as the Sesia-Lanzo Zone show post eclogite-peak cooling already at high pressures, similar to our results, whereas structurally deeper, westerly units (Dora Maira, Gran Paradiso, Monte Rosa) show decompression either at isothermal conditions or slightly increasing temperatures (POGNANTE, 1991). These *P-T* paths can be linked to processes in an imbricated subduction setting such as rapid underthrusting and thermal interaction between these thin slabs in a nappe stack (POGNANTE, 1989b).

Acknowledgments

This work was supported by NSF grants EAR 92-05649 and EAR 95-26596 to EJE, as well as a fellowship from the Austrian Bundesministerium für Wissenschaft und Forschung, and grants from the International Institute of the University of Michigan, Turner Fund of the Department of Geological Sciences at the University of Michigan, and the Geological Society of America to the first author. Carl Henderson is thanked for his help with the electron microprobe and the scanning electron microscope at the Electron Microbeam Analysis Laboratory (EMAL) at the University of Michigan. The authors are grateful to Guido Venturini and Giovanni Armando for their help in the field, and to Mag. Rainhard Kaindl for performing Micro-Raman spectroscopy

on fine kyanite inclusions in eclogite-facies garnets. The authors wish to thank Gaston Godard and an anonymous reviewer for their constructive and thorough reviews which considerably helped to improve the manuscript. Comments of two anonymous reviewers on an earlier version of the manuscript are also gratefully acknowledged.

References

AFIFI, A. and ESSENE, E.J. (1988): MINFILE, a microcomputer program for storage and manipulation of chemical data on minerals. Am. Mineral. 73, 446–448.

ARMANDO, G. (1992): Studio geologico dell'alta valle dell'Elvo (Zona Sesia-Lanzo, Alpi Occidentali). MSc Thesis, University of Torino, 196 pp.

AUSTRHEIM, H. (1987): Eclogitization of lower crustal granulites by fluid migration through shear zones. Earth Planet. Sci. Lett. 81, 221–232.

AYERS, J.C. and WATSON, B.E. (1993): Rutile mobility in supercritical aqueous fluids. Contrib. Mineral. Petrol. 114, 321–330.

BARNICOAT, A.C. (1988): The mechanism of veining and retrograde alteration of Alpine eclogites. J. Metamorphic Geol. 6, 545–558.

BARNICOAT, A.C. and CARTWRIGHT, I. (1995): Focused fluid flow during subduction: Oxygen isotope data from high-pressure ophiolites of the Western Alps. Earth Planet. Sci. Lett. 132, 53–61.

BEARTH, P. (1967): Die Ophiolithe der Zone von Zermatt-Saas Fee. Beiträge zur Geologischen Karte der Schweiz, 132 pp.

CARSWELL, D.A., (1990): Eclogites and the eclogite-facies: definitions and classifications. In: CARSWELL, D.A. (ed.): Eclogite-facies Rocks, Blackie, New York, 1–13.

CHINNER, G.A. and DIXON, J.E. (1973): Some high-pressure parageneses of the Allalin Gabbro, Valais, Switzerland. J. Petrol. 14, 185–202.

COMPAGNONI, R., LOMBARDO, B., MESSIGA, B. and TRIBUZIO, R. (1993): The eclogites in the continental crust of the Western Alps. In: MORTEN, L. (ed.): Italian Eclogites and Related Rocks, Accademia Nazionale delle Scienze Detta Dei XL, Roma, 59–78.

COMPAGNONI, R., DAL PIAZ, G.V., HUNZIKER, J.C., GOSSO, G., LOMBARDO, B and WILLIAMS, P.F. (1977): The Sesia-Lanzo Zone, a slice of continental crust with Alpine high pressure-low temperature assemblages in the western Italian Alps. Rend. Soc. Ital. Mineral. Petrol. 33, 281–334.

DAL PIAZ, G.V., HUNZIKER, J.C. and MARTINOTTI, G. (1972): La Zona Sesia-Lanzo e l'evoluzione tectonico-metamorphica della Alpi nordoccidentali interne. Mem. Soc. Geol. Ital. 11, 433–466.

DONOHUE, C.L. and ESSENE, E.J. (2000): An oxygen barometer with the assemblage garnet-epidote. Earth Planet. Sci. Lett. 181, 459–472.

DUCHÊNE, S., BLICHERT-TOFT, J., LUAIS, B, TÉLOUK, P., LARDEAUX, J.M. and ALBAREDE, F. (1997): The Lu-Hf dating of garnets and the ages of the Alpine high-pressure metamorphism. Nature 387, 586–589.

EVANS, B.W. (1990): Phase relations of epidote-blueschists. Lithos 25, 3–23.

FRANZ, G., THOMAS, S. and SELVERSTONE, J. (1989): Fluid in eclogites: evidence from high-pressure veins in the Austrian Alps. Eos 70, 1377.

GANGULY, J., WEIJI, C. and TIRONE, M. (1996): Thermodynamics of aluminosilicate garnet solid solution: new experimental data, an optimized model and thermometric applications. Contrib. Mineral. Petrol. 126, 137–151.

GETTY, S.R. and SELVERSTONE, J. (1994): Stable isotopic and trace element evidence for restricted fluid migration in 2 GPa eclogites. J. Metamorphic Geol. 12, 747–760.

GIORGETTI, G., TROPPER, P., ESSENE, E.J. and PEACOR, D.R. (2000): Characterization of coexisting non-equilibrium and equilibrium paragonite/muscovite intergrowths in an eclogite from the polymetamorphic Sesia-Lanzo Zone (Western Alps, Italy). Contrib. Mineral. Petrol. 138, 326–336.

GRAHAM, C.M. and POWELL, R. (1984): A garnet-hornblende geothermometer: calibration, testing, and application to the Pelona Schist, Southern California. J. Metamorphic Geol. 2, 13–31.

GREEN, N.L. and USDANSKY, S.I. (1986): Toward a practical plagioclase-muscovite thermometer. Am. Mineral. 71, 1109–1117.

HAÜY, R.J. (1822): Traité de Minéralogie. 2nd Edition, Bachelier, Paris Delance, IV, 584 pp.

HENRY, C., BURKHARD, M. and GOFFE, B. (1996): Evolution of synmetamorphic veins and their wallrocks through a Western Alps transect: no evidence for large-scale fluid flow. Stable isotope, major- and trace-element systematics. Chem. Geol. 127, 81–109.

HOLLAND, T.J.B. (1990): Activities of components in omphacitic solid solutions. An application of Landau theory to mixtures. Contrib. Mineral. Petrol. 105, 446–453.

HOLLAND, T.J.B. and POWELL, R. (1998): An internally consistent thermodynamic data set for phases of petrological interest. J. Metamorphic Geol. 8, 89–124.

HOLLAND, T.J.B. and POWELL, R. (1991): A compensated Redlich-Kwong (CORK) equation for volumes and fugacities of CO_2 and H_2O in the range of 1 bar to 50 kbar and 100–1600 °C. Contrib. Mineral. Petrol. 109, 265–273.

HUNZIKER, J.C. (1974): Rb–Sr and K–Ar age determination and the Alpine tectonic history of the Western Alps. Mem. Sci. Geol. (Univ. Padova) 31, 1–55.

INGER, S., RAMSBOTHAM, W., CLIFF, R.A. and REX, D.C. (1996): Metamorphic evolution of the Sesia-Lanzo Zone, Western Alps: time constraints from multi-system geochronology. Contrib. Mineral. Petrol. 126, 152–168.

JAMTVEIT, B. and YARDLEY, B.W.D. (1997): Fluid Flow and Transport in Rocks. London, Chapman and Hall, 450 pp.

KRETZ, R. (1983): Symbols for rock-forming minerals. Am. Mineral. 68, 277–279.

KROGH RAVNA, E. J. (2000a): The garnet-clinopyroxene Fe^{2+}–Mg geothermometer: an updated calibration. J. Metamorphic Geol. 18, 211–219.

KROGH RAVNA, E. J. (2000b): Distribution of Fe^{2+} and Mg between coexisting garnet and hornblende in synthetic and natural systems: an empirical calibration of the garnet-hornblende Fe-Mg thermometer. Lithos 53, 265–277.

LARDEAUX, J.M., GOSSO, G., KIENAST, J.R. and LOMBARDO, B. (1982): Relations entre le métamorphisme et la déformation dans la zone de Sésia-Lanzo (Alpes occidentales) et le problème de l'éclogitisation de la croûte continentale. Bull. Soc. Géol. France 24, 793–800.

LEAKE, B.E. et al. (1997): Nomenclature of amphiboles: report of the subcommittee on amphiboles of the international mineralogical association, commission on new minerals and mineral names. Can. Mineral. 35, 219–246.

LIU, J., BOHLEN, S.R. and ERNST, W.G. (1996): Stability of hydrous phases in subducting oceanic crust. Earth Planet. Sci. Lett. 143, 161–171.

MARUYAMA, S., LIOU, J.G. and TERABAYASHI, M. (1996): Blueschists and eclogites of the world and their exhumation. Int. Geol. Rev. 38, 485–594.

MARUYAMA, S., CHO, M. and LIOU, J.G. (1986): Experimental investigations of blueschist-greenschist transition equilibria: pressure dependence of Al_2O_3 contents in sodic amphiboles – a new geobarometer. In: EVANS, B.W. and BROWN, E.D. (eds): Blueschists and Eclogites. Geol. Soc. Am. Mem. 164, 1–17.

MILLER, C. (1974): Reaction rims between olivine and plagioclase in metaperidotites, Ötztal Alps. Contrib. Mineral. Petrol. 43, 333–342.

MILLER, C. and THÖNI, M. (1997): Eo-Alpine eclogitisation of Permian MORB-type gabbros in the Koralpe (Eastern Alps, Austria): new geochronological, geochemical and petrological data. Chem. Geol. 137, 283–310.

MOLINA, J.F. and POLI, S. (2000): Carbonate stability and fluid composition in subducted oceanic crust: an experimental study on H_2O–CO_2-bearing basalts. Earth Planet. Sci. Lett. 176, 295–310.

NADEAU, S., PHILIPPOT, P. and PINEAU, F. (1993): Fluid inclusion and mineral isotopic compositions (H–C–O) in eclogitic rocks as tracers of local fluid migration during high-pressure metamorphism. Earth Planet. Sci. Lett. 114, 431–448.

OBERHÄNSLI, R., HUNZIKER, J.C., MARTINOTTI, G. and STERN, W.B. (1985): Geochemistry, geochronology and petrology of Monte Mucrone: an example of Eo-Alpine eclogitization of Permian granitoids in the Sesia-Lanzo Zone, Western Alps, Italy. Chem. Geol. 52, 165–184.

PASSCHIER, C.W., URAI, J.L., VAN LOON, J. and WILLIAMS, P.F. (1981): Structural geology of the central Sesia Lanzo Zone. Geologie en Mijnbouw 60, 497–507.

PEACOCK, S.M. (1993): The importance of blueschist-eclogite dehydration reactions in subducting oceanic crust. Geol. Soc. Am. Bull. 105, 684–694.

PHILIPPOT, P. (1987): "Crack-seal" vein geometry in eclogitic rocks. Geodinamica Acta (Paris) 1, 171–181.

PHILIPPOT, P. and SELVERSTONE, J. (1991): Trace-element-rich brines in eclogitic veins: implications for fluid composition and transport during subduction. Contrib. Mineral. Petrol. 106, 417–430.

PHILIPPOT, P., CHEVALLIER, P., CHOPIN, C. and DUBESSY, J. (1995): Fluid composition and evolution in coesite-bearing rocks (Dora-Maira Massif, Western Alps): implications for element recycling during subduction. Contrib. Mineral. Petrol. 121, 29–44.

POGNANTE, U. (1991): Petrological constraints on the eclogite- and blueschist-facies metamorphism and P-T-t paths in the Western Alps. J. Metamorphic Geol. 9, 5–17.

POGNANTE, U. (1989a): Lawsonite, blueschist and eclogite formation in the southern Sesia zone (western Alps, Italy). Eur. J. Mineral. 1, 89–104.

POGNANTE, U. (1989b): Tectonic implications of lawsonite formation in the Sesia zone (Western Alps). Tectonophysics 162, 219–227.

POGNANTE, U., COMPAGNONI, R. and GOSSO, G. (1980): Microstructural relationships in the continental eclogitic rocks of the Sesia-Lanzo Zone: a record of a subduction cycle. Rend. Soc. It. Miner. Petrogr. 36, 169–186.

REINSCH, D. (1979): Glaucophanites and eclogites from Val Chiusella, Sesia-Lanzo Zone (Italian Alps). Contrib. Mineral. Petrol. 70, 257–266.

RUBATTO, D., GEBAUER, D. and COMPAGNONI, R. (1999): Dating of eclogite-facies zircons: the age of Alpine metamorphism in the Sesia-Lanzo Zone (Western Alps). Earth Planet. Sci. Lett. 167, 141–158.

SELVERSTONE, J., FRANZ, G., THOMAS, S. and GETTY, S. (1992): Fluid variability in 2 GPa eclogites as an indicator of fluid behavior during subduction. Contrib. Mineral. Petrol. 112, 341–357.

TROPPER, P., ESSENE, E.J., SHARP, Z.D. and HUNZIKER, J.C. (1999): Application of K-feldspar-jadeite-quartz barometry to eclogite-facies metagranites and metapelites in the Sesia Lanzo Zone (Western Alps, Italy). J. Metamorphic Geol. 17, 195–209.

VENTURINI, G. (1995): Geology, geochemistry and geochronology of the inner central Sesia Zone (Western Alps-Italy), Mém. Géol. (Lausanne) 25, 147 pp.

VENTURINI, G., MARTINOTTI, G., ARMANDO, G., BARBERO, M. and HUNZIKER, J.C. (1994): The Central Sesia-Lanzo Zone (Western Italian Alps): new field observations and lithostratigraphic subdivisions. Schweiz. Mineral. Petrogr. Mitt. 74, 111–121.

Manuscript received April 4, 2001; revision accepted September 20, 2002.
Editorial handling: I. Spalla

Appendix 1: Analytical conditions

Electron microprobe analyses of the minerals were obtained on a CAMECA CAMEBAX microprobe with four wavelength dispersive spectrometers (WDS) at the University of Michigan. Natural and synthetic phases were used as standards: Tiburon albite (Na), Gotthard adularia (K), New Idria jadeite (Na), synthetic diopside (Si), Broken Hill rhodonite (Mn), synthetic uvarovite (Cr), Ingamells almandine (Fe, Al), synthetic geikelite (Ti), Marjalahti olivine (Mg), Mariposa Co. sanbornite (Ba), Topaz Mts. topaz (F), synthetic Ba-Cl apatite (Cl) and Willsboro wollastonite (Ca). Analyses were obtained at 15 kV and 10 nA with a focused beam except for feldspars, Na-amphiboles and micas, which were analyzed with a 3 mm^2 beam to minimize volatilization of alkali elements. The carbonates were analyzed with a reduced voltage of 10 kV to avoid beam damage. Counting times were 20 s for most elements, except for F in titanite which was analyzed with 50 s. The raw data were reduced with a PAP type correction, provided by CAMECA, and the stoichiometric mineral formulas were calculated using the program MINFILE (AFIFI and ESSENE, 1988).

Appendix 2: Equilibria used in the *P-T-a*(H_2O) calculations

Inclusion assemblage in garnet core (high-pressure stage I)

Equilibria for P-T constraints:

4 Lawsonite = 2 Clinozoisite/Zoisite + Kyanite + Quartz + 7 H_2O (1a,b)
3 Anorthite = Grossular + 2 Kyanite + Quartz (2)
2 Clinozoisite/Zoisite + Kyanite + Quartz = 4 Anorthite + H_2O (3a,b)
Clinozoisite/Zoisite = Grossular + Kyanite + Quartz + H_2O (4a,b)
Grossular + Paragonite + Kyanite + Quartz = Clinozoisite/Zoisite + Jadeite (5a,b)
Jadeite + Kyanite + H_2O = Paragonite (6)

Inner garnet rim inclusion assemblage (high-pressure stage II)

Equilibria for H_2O-free P-T constraints:

Grossular + Pyrope + 2 Quartz = 3 Diopside + 2 Kyanite (7a)
Grossular + Almandine + 2 Quartz = 3 Hedenbergite + 2 Kyanite (7b)
Almandine + 3 Diopside = Pyrope + 3 Hedenbergite (8)

Equilibria for a(H_2O) constraints:

15 Diopside + 12 Clinozoisite = 13 Grossular + 5 Pyrope + 12 Quartz + 6 H_2O (9)
6 Clinozoisite = 4 Grossular + 5 Kyanite + Quartz + 3 H_2O (10)
4 Pyrope + 6 Clinozoisite + 7 Quartz = 12 Diopside + 13 Kyanite + 3 H_2O (11)
6 Clinozoisite = 4 Grossular + 5 Kyanite + Quartz + 3 H_2O (12)
15 Hedenbergite + 12 Clinozoisite = 13 Grossular + 5 Almandine + 12 Quartz + 6 H_2O (13)
4 Almandine + 6 Clinozoisite + 7 Quartz = 12 Hedenbergite + 13 Kyanite + 3 H_2O (14)

Late eclogite facies matrix assemblage (high-pressure stage III)

Equilibria for P-T constraints:

15 Diopside + 12 Clinozoisite = 13 Grossular + 5 Pyrope + 12 Quartz + 6 H_2O (15)
15 Hedenbergite + 12 Clinozoisite = 13 Grossular + 5 Almandine + 12 Quartz + 6 H_2O (16)
3 Hedenbergite + Pyrope = 3 Diopside + Almandine (17)
Jadeite + Quartz = Albite (18)

Equilibria for X(H_2O)-X(CO_2) constraints:

Diopside + 2 CO_2 = Dolomite + 2 Quartz (19)
15 Diopside + 12 Clinozoisite = 13 Grossular + 5 Pyrope + 12 Quartz + 6 H_2O (20)
13 Grossular + 5 Pyrope + 30 CO_2 + 6 H_2O = 12 Clinozoisite + 18 Quartz + 15 Dolomite (21)

Blueschist-facies assemblage

Equilibria for P-T constraints:

25 Glaucophane + 6 Clinozoisite + 14 H_2O + 7 Quartz = 9 Clinochlore + 6 Tremolite + 50 Albite (22)
2 Albite + 6 Lawsonite + 3 Pumpellyite = 9 Clinozoisite + Glaucophane + + Quartz + 17 H_2O (23)

Greenschist-facies assemblage

Equilibria for P-T constraints:

2 Clinochlore + 5 Prehnite + 2 Quartz = 4 Clinozoisite +Tremolite + 6 H_2O (24)
2 Clinochlore + 25 Pumpellyite + 29 Quartz = 43 Clinozoisite + 7 Tremolite + 67 H_2O (25)
Clinochlore + 6 Clinozoisite + 7 Quartz = Tremolite + 10 Anorthite + 6 H_2O (26)

Equilibria for X(H_2O)-X(CO_2) constraints:

3 Dolomite + 4 Quartz + H_2O = 3 Calcite + Talc + 3 CO_2 (27)
5 Talc + 6 Calcite + 4 Quartz = 3 Tremolite + 2 H_2O + 6 CO_2 (28)